Structural Basis and Mechanism of TrkA Activation by NGF through Ligand-Induced Rotation of Transmembrane Domain Dimers

María L. Franco[1,4], Kirill D. Nadezhdin[2,3,4], Sergey A. Goncharuk[2,3], Konstantin S Mineev[2,3], Alexander S. Arseniev[2,3]* and Marçal Vilar[1]*

[1]Molecular Basis of Neurodegeneration Unit. Institute of Biomedicine of València (IBV-CSIC). C/ Jaume Roig 11, 46010 València, Spain.

[2]Shemyakin-Ovchinnikov Institute of Bioorganic Chemistry of the Russian Academy of Sciences, Moscow 117997, Russian Federation.

[3]Moscow Institute of Physics and Technology (State University), Institutskiy Pereulok 9, Dolgoprudny, Moscow Region 141700, Russian Federation.

[4]Co-First author.

*co-corresponding authors: aars@nmr.ru , mvilar@ibv.csic.es

Running Title: Mechanism of Activation of TrkA by NGF

Abstract

Trk receptors are essential for the nervous system development. The molecular mechanism of TrkA activation by its ligand NGF is still unsolved. Recent data indicates that at endogenous levels most of TrkA is in an equilibrium monomer-dimer and the binding of NGF induces an increase of the dimer and oligomer forms of the receptor. An unsolved issue is the role of the transmembrane domain (TMD) in the dimerization of TrkA and the structural details of the TMD in the active dimer receptor. We found that TrkA-TMD can form dimers, identified the structural determinants of the dimer interface in the active receptor and validated this interface using site-directed mutagenesis together with functional and cell differentiation studies. As around 20% of TrkA is in an inactive dimeric form in the absence of ligand how NGF binding is able to active this pre-formed dimer is unknown. Using *in vivo* crosslinking we identified a reordering of the extracellular juxtamembrane (JTM) region after ligand binding. This conformational change could be mimicked by replacement of some residues in the JTM with cysteine that form ligand-independent active dimers and reveal a preferred dimer interface. In addition to that, insertion of leucine residues into the TMD helix induces a ligand-independent TrkA activation suggesting that a rotation of the TMD dimers could be behind TrkA activation by NGF. Altogether our data indicate that the transmembrane and juxtamembrane regions of the receptor play a key role in the dimerization and conformational activation of TrkA by NGF.

50 **Introduction**

51 Nerve growth factor (NGF) is a member of the mammalian neurotrophin (NT) protein
52 family implicated in the maintenance and survival of the peripheral and central nervous
53 systems (1-3). NGF is a dimer that interact with two distinct receptors, TrkA a cognate
54 member of the Trk receptor tyrosine kinase family and the p75 neurotrophin receptor,
55 which belongs to the tumor necrosis factor receptor (TNFR) superfamily of death receptors
56 (4-6). TrkA signalling is essential for sensory and sympathetic neuron survival during
57 development (7). Genetic mutations in the NTRK1 gene cause Congenital Insensitivity to
58 Pain with Anhidrosis (CIPA), a rare disease (8), and somatic mutations and chromosomal
59 rearrangements generate aberrant protein fusions with constitutive kinase activation causing
60 several types of cancer (9, 10).

61 Despite all these important roles, the molecular mechanisms of TrkA activation have been
62 poorly studied in comparison with those of other receptor tyrosine kinase (RTK) family
63 members (11, 12). The first three extracellular domains of TrkA consist of a leucine-rich
64 region, LRR (Trk-d1) that is flanked by two cysteine-rich domains (Trk-d2 and Trk-d3).
65 The fourth and fifth domains (Trk-d4 and Trk-d5) are immunoglobulin (Ig)-like domains,
66 and these are followed by a 30-residue-long linker that connects the extracellular portion of
67 the receptor to the single transmembrane domain and a juxtamembrane intracellular region
68 that is connected to the kinase domain. TrkA is activated by nerve growth factor (NGF) a
69 member of the neurotrophin family (3). The NGF binding domain is located in the Trk-
70 d5(Ig2) domain (13) although other domains also participate in activation by NTs through
71 an unknown mechanism (14, 15).

72 Two models for TrkA activation are postulated; a ligand-induced dimerization of TrkA
73 monomers and a ligand-induced conformational activation of pre-formed inactive dimers.
74 The first model, which is based on the crystal structure of NGF with the ligand-binding

75 domain of TrkA (13, 16), assumed that the dimerization of TrkA is solely ligand-mediated
76 and that receptor-receptor interactions are not present in the absence of its ligand. In the
77 second model TrkA exists as a pre-formed inactive dimer suggesting receptor-receptor
78 contacts in the absence of NGF (17, 18). The most recent data using single-particle tracking
79 (19) and FRET studies (20) suggests that TrkA is, at endogenous levels, predominantly
80 monomer (80%) and NGF binding induces an increase and a stabilization of the TrkA
81 dimers and the formation of oligomers, together with a conformational change leading to
82 kinase activation. This mechanism of activation has been called the "transition model" (20)
83 and postulates a dynamic transition from a monomer to an inactive dimer to a ligand-bound
84 active dimer, suggesting that Trk receptors are activated through a combination of the two
85 mentioned models.
86 Whatever the model, it is clear that dimerization of TrkA is required for its activation.
87 Deletion constructs suggested that dimerization of TrkA in the absence of NGF is mediated
88 by the transmembrane (TM) and by the intracellular domains (ICD) (20). In the case of the
89 ICD this is supported by the crystal structure of the kinase domain of TrkA that showed the
90 presence of dimers in the crystallographic unit (21, 22). However the structural determinants
91 of the TMD dimerization are not know and in this regard, it is important to understand the
92 conformation of the TrkA-TMD dimer and identify the active dimer interface that may
93 represent the functional state of the full-length receptor. In addition biochemical data
94 supporting a conformational activation of TrkA pre-formed dimers are lacking.

95 In the present work we investigated the role of TrkA-TMDs in its activation, using several
96 complementary structural and molecular biological approaches. Here we present the
97 structure of the dimeric TMD in the receptor active state and show that the coupling of
98 ligand-binding to rotation of the TMD may underlie the TrkA activation by NGF.

99

100 **Results**

101 **Structural basis of TrkA transmembrane domain dimerization.**

102 It has been shown that the isolated TMDs of all human RTKs form dimers in bacterial
103 membranes (23). In addition functional studies indicate that TMDs play an important role
104 as a modulator of RTK homodimerization and kinase activation (reviewed in (23-25)).
105 Switching between two dimerization modes of the transmembrane helix has recently been
106 described as part of the activation mechanism of the EGF, VEGF and FGF receptors (26-
107 29). However, to date the role of TrkA-TMD dimerization in TrkA receptor activation has
108 not been studied in detail. Here we used two different approaches to characterize the
109 dimerization of the TrkA-TMD. First, to study TrkA-TMD dimerization in a biological
110 membrane context we used ToxRED, a genetic bacterial system, to assess TrkA
111 transmembrane dimerization using ToxCAT as a reporter system (30, 31). The TrkA-TMD
112 self-associated in biological membranes in this system (Figure 1A). To determine the TrkA
113 amino acid residues implicated in this dimerization we assayed the effect in this assay of
114 individual mutation of each of the small residues (Ala, Gly or Ser) in the TMD sequence to
115 a bulky residue such as isoleucine. This approach to disruption of dimerization was similar
116 to that used in classical studies of glycophorin-A, in which the mutation G83I impaired its
117 TMD dimerization (31). In our study, less TMD dimerization was observed in the S419I
118 and G423I mutants compared to wt (Figure 1B), implicating the sequence $S_{419}xxxG_{423}$ as
119 part of the TrkA-TMD dimerization motif in bacterial membranes.

120 To obtain a structural insight into TrkA-TMD dimerization we solved the structure of
121 human TrkA-TMD dimers in lipid micelles using NMR. For this study, the human TrkA-
122 TMD was produced in a cell-free system (see Experimental Procedures) as previously
123 described (32). When the peptide is solubilized in dodecylphosphocholine (DPC) micelles

124 at a lipid-to-protein molar ratio (LPR) of 50:1 the TrkA-TMD is in equilibrium between
125 monomeric, dimeric and other oligomeric states. The ratio of these states varies as the LPR
126 value is altered (Figure S1A). We then titrated TrkA-TMD in DPC micelles using a
127 standard technique in our laboratory (33) to measured the standard free energy of
128 dimerization (ΔG_0) (Figure S1B). The ΔG_0 value obtained (-1.9±0.2 kcal/mol) suggested
129 that the TrkA-TMD dimer is quite stable compared to the TMD dimers of other RTKs.
130 Thus, although its dimerization energy is weaker than that of the VEGFR2 dimer (ΔG_0 = -
131 2.5 kcal/mol in DPC) (34), it is stronger than that of FGFR3 (ΔG_0 = -1.4 kcal/mol in
132 DPC/SDS 9:1 mixture) and ErbB4 (ΔG_0 = -1.4 kcal/mol in DMPC/DHPC 1:4 bicelles)
133 (35). The ^{15}N-HSQC spectrum of ^{15}N labeled-TrkA-TMD (Figure S2) contained the
134 expected number of cross-peaks, and the good quality of the spectra allowed solving of the
135 structure of the dimer in DPC micelles (Figures 1C, Figure S3, Figure S4, Figure S5 and
136 Table S1). The α-helical region of the TrkA-TM dimer starts at G417, ends at N440, and is
137 ~38 Å in length (Figure S3). The crossing angle of the TrkA-TM helices is 40º, and the
138 minimal distance between two monomers is 8.8 Å (Figure 1C and Table S1). The
139 hydrophobicity plot and contact surface area of the dimer is shown in Figure S5. The
140 dimerization interface lies along the sequence motif $L_{424}xxF_{427}A_{428}xxF_{431}$ (Figure 1C and
141 Figure S5) that is conserved in the TrkA-TMD of several species and also in TrkC but not
142 in TrkB (Figure 1D).
143 These analyses of TrkA-TMD dimerization suggested the existence of two possible
144 dimerization motifs; $S_{419}xxxG_{423}$ and $L_{424}xxF_{427}A_{428}xxF_{431}$, which are located on opposite
145 faces of the TMD helix (Figure 1C). The latter motif was found in analysis of the
146 dimerization of TMDs in micelles using a direct approach and in the context of the isolated
147 domain, while the former motif was observed in analysis of the dimerization of TMDs in

148 real membranes, using an indirect approach and in the context of a chimeric protein. Thus,
149 the biological relevance of each motif can be questioned, as the presence of large
150 extracellular and intracellular globular domains or the lipid environment of the plasma
151 membrane may favour or hinder a specific interaction interface (36). We therefore used
152 different functional assays to verify the found dimer interfaces in the context of the full-
153 length receptor.
154
155 **Functional identification of the dimer interface upon NGF stimulation.**
156 The state of full-length TrkA was followed by assay of three different aspects of its
157 activity: dimerization of the receptor, phosphorylation of intracellular tyrosine residues and
158 neurite differentiation of PC12nnr5 cells. To investigate the dimerization of TrkA, we
159 individually mutated most of the N-terminal residues of the rat TrkA-TMD to cysteine
160 (Figure 2A), expressed these constructs in Hela cells, and then measured the amount of
161 cross-linked species. To facilitate cross-linking via these cysteine residues in the
162 transmembrane domains we used oxidation with molecular iodine (I_2) as previously
163 described (37). Such oxidation allows the formation of a disulfide bond between two close
164 cysteine residues inside the lipid bilayer. Plasma membrane fractions from cells expressing
165 different single-cysteine mutants were incubated in the absence or presence of NGF,
166 together with molecular I_2 and were then analyzed by non-reducing SDS-PAGE and
167 western immunoblotting. As shown in Figures 2B and 2C the mutants F416C, G417C and
168 A421C formed covalent dimers in the absence of NGF. Upon NGF stimulation the amount
169 of F416C, G417C and A421 dimers increased and a dimer was newly seen in the V418C
170 mutant (Figures 2B and 2C). The residues G417, F416 and A421 are very close to each
171 other in the NMR structure (Figures 2D and 2E), supporting the NMR-derived
172 conformation as the active state of the TrkA dimer.

173 To further study the significance of the found interfaces, we mutated the small residues Ala,
174 Gly and Ser within this region to the bulky Ile residue and we then assayed TrkA activation
175 upon NGF stimulation (Figures 2F and 2G). The rationale behind this approach was that the
176 mutation of a small residue to a bulky one on the relevant interface would prevent the
177 formation of the active dimeric state by inducing steric clashes, and would, therefore,
178 reduce TrkA activation. To perform this assay, we transfected Hela cells that do not express
179 endogenous TrkA with these mutants, stimulated these cells with non-saturating
180 concentrations (10 ng/mL) of NGF, and then assayed TrkA activation by analysis of TrkA
181 autophosphorylation using western blotting. Upon transfection, two TrkA electrophoretic
182 bands are present in the TrkA immunoblots of Hela cells; a lower band (approx.110 kDa) of
183 intracellular immature TrkA that has not completed Golgi-mediated processing of high-
184 mannose N-glycans (38) and an upper band (approx.140 kDa) with mature sugars that is
185 expressed in the plasma membrane. Exposure to NGF substantially increased the
186 phosphorylation of the upper TrkA band as assessed by blotting with a phospho-specific
187 antibody against the phospho-tyrosine residues of the activation loop, Tyr674 and Tyr675
188 (P-Y674/5). This autophosphorylation was quantified to follow TrkA activation.
189 Constitutive (t=0, no NGF added) and ligand-dependent phosphorylation of plasma
190 membrane-localized TrkA after 5 and 15 minutes were measured. Since overexpression of
191 TrkA induces ligand-independent autophosphorylation, we first transfected the Hela cells
192 with increasing concentrations of TrkA to determine a TrkA level that could still be
193 detected but that displayed no autophosphorylation in the upper band in the absence of
194 NGF (Figure S6). It is noteworthy that all mutants are expressed at the plasma membrane as
195 evidenced by both immunofluorescence localization in the absence of Triton X-100 using
196 an antibody against an epitope in the TrkA N-terminus (Figure S7) and by flow cytometry
197 (Figure 2H). Out of the seven single-point mutants tested only the A428I substitution

198 demonstrated a pronounced inhibitory effect on receptor autophosphorylation. A428 is the
199 only small-chain residue that is found deep in the dimerization interface of the TrkA TMD
200 conformation determined using NMR, which further supports the relevance of the obtained
201 NMR structure. The inhibitory effect of A428 substitution on receptor activity was further
202 enhanced when all three Ala residues that are at least somehow involved in the TMD
203 dimerization in the NMR-based structure, A421, A425 and A428, were simultaneously
204 substituted (TrkA-3A/3I).
205 Lastly, we studied the effect of the same mutations on the NGF-induced differentiation of
206 transfected PC12nnr5 cells (Figure 2H). Again, the A428I mutant displayed substantial
207 inhibition of this TrkA activity. Unexpectedly, although the mutation S419I had no effect
208 on TrkA activation by NGF in these two assays, the mutation G423I did have an impact on
209 cell differentiation (Figure 2H). This result suggested that G423 is located at a helix
210 interface that is important in the downstream activation and signalling of TrkA leading to
211 cell differentiation (See Discussion).
212 The combined results of the functional assays agree regarding the importance of the NMR-
213 derived TMD structure for TrkA activation. The critical role of the residue A428 in TrkA
214 activation by NGF together with its location deep in the dimer interface indicates that the
215 NMR-based structure corresponds to the mode of TMD interaction in the NGF-induced
216 active state of the receptor
217
218 **A specific conformation of extracellular juxtamembrane residues is necessary for**
219 **TrkA activation.**
220 Stimulation of Hela cells transfected with TrkA-wt with NGF induces the formation of
221 TrkA dimers that are crosslinked with BS3 (Figure 3). While it is known that TrkA dimers
222 are formed in the absence of NGF, no cross-linking was observed without the ligand, which

223 suggests that ligand binding is accompanied by changes in the conformation of the
224 extracellular part of the protein. As BS3 reacts only with free amines (the side-chains of
225 Lys residues or a free N-terminus) we searched for possible sites in TrkA that might have
226 caused the observed crosslinking. According to the crystal structure of the TrkA/NGF
227 complex (15) (Figure 3A), there are no lysine residues in the TrkA-ECD that are located in
228 a position where crosslinking of the side chains of Lys residues of two monomers could
229 occur. Since BS3 does not cross the plasma membrane, and since we used the full-length
230 TrkA receptor in our assays, we wondered if the observed BS3 cross-linking was mediated
231 via crosslinking of K410 and K411 in the extracellular juxtamembrane region (eJTM) of
232 TrkA (Figure 3A) since this region is not observed in the crystal structure (16). To verify
233 this hypothesis, we mutated both K410 and K411 to Arg and repeated the initial experiment
234 using HEK293 cells transfected with this TrkA-KK/RR construct (Figure 3B). No BS3-
235 induced TrkA crosslinking was observed in the TrkA-KK/RR-transfected cells suggesting
236 that NGF binding brings this region of the eJTM into close proximity.
237 We considered that, if NGF indeed induces contacts between these eJTM regions, then we
238 should be able to mimic this activity of NGF by forcing the dimerization of eJTMs in the
239 absence of NGF. For this purpose, we individually mutated most of the residues in the
240 eJTM of TrkA to cysteine and subsequently analyzed the dimerization of these transfected
241 single point mutants (Figure 4A). After transfection of Hela cells, disulfide dimers were
242 spontaneously formed in all constructs but the amount of dimers differed between the
243 various mutants (Figure 4B). The amount of dimer is significantly higher in the positions
244 D412C and K411C. As a functional assay we then transfected these mutants into HeLa
245 cells, which do not express endogenous TrkA, and quantified the phosphorylation of the
246 tyrosines from the kinase activation loop (Y674/675) in the absence and presence of NGF
247 (Figure 4C). This analysis showed the presence of active dimers (D406C, K410C and

248 K411C) which are activated constitutively in the absence of NGF, and dimers that are not
249 active in the absence of NGF (V408C, D412C, E413C and T414C). In general there is a
250 poor correlation (Figure 4D) between the amount of dimer formation and constitutive
251 activation, suggesting that dimerization by itself is not enough for TrkA activation.
252 However the mutants with higher constitutive activation (D406C, K410C and K411C)
253 showed a good correlation between dimer formation and activation (Figure 4D, green dots,
254 r^2=0.92). We then transfected some of the active mutants in PC12nnr5 cells. In the absence
255 of NGF the R405C, K410C and K411C mutants induced the formation of neurites in
256 PC12nnr5 cells (Figures 4E and 4F) supporting the constitutive activation of these mutants
257 and suggested that disulfide bond formation through this interface mimics the binding of
258 NGF. If we assume that the TMD α-helix continues in the juxtamembrane region the
259 residues R405, K410 and K411 are in one face of the helix (in green in the Figure 4G). By
260 contrast the residues whose mutation to cysteine induces inactive dimers are located in
261 another face (in red in the Figure 4G). All the mutants are correctly expressed at the plasma
262 membrane as found by flow cytometry (Figure 4H).
263 In the presence of NGF these mutants showed no further activation by NGF (Figure 4C)
264 suggesting they are fully active and the dimer interface adopted by the cysteine dimers is
265 similar or identical to the one obtained with NGF binding. By contrast the mutants that
266 form inactive dimers respond to NGF in a similar manner or even higher than the wt
267 (Figure 4C), indicating that covalent dimer formation do not preclude the activation by the
268 ligand. How can NGF activate a covalent dimer if the cysteine are located downstream of
269 the ligand binding domain? The most plausible explanation is that NGF can induce the
270 dimerization of two pre-formed inactive dimers as shown in the Figure 4H.

271 In summary, our results supports the notion of the insufficiency of TrkA dimerization alone
272 for receptor activation and support the existence of an preferred active dimer interface that
273 continues through the TMD.
274
275 **An Induced rotation activates TrkA in the absence of NGF**
276 It is known that overexpression of TrkA induce a ligand-independent activation of TrkA.
277 However the levels of autophosphorylation are lower than in the presence of NGF. The
278 western blotting shown in Figure 5A shows the autophosphorylation of the intracellular
279 tyrosines of TrkA (Tyr-674/5, Tyr-490 and Tyr-751) and downstream signaling (P-ERK)
280 due to TrkA overexpression (absence of NGF) and in the presence of NGF. The blots
281 indicate that, although the overexpression of TrkA induces a ligand-independent activation
282 (probably by facilitating receptor dimerization), the presence of NGF is required for a
283 higher and complete activation of the receptor. The complete sequence of the events caused
284 by the ligand is also of great importance for receptor activation. As we have shown above,
285 ligand binding brings eJTM regions into proximity at certain specific positions. In turn,
286 such proximity can either result in a mutual rotation of the receptor TMDs or change the
287 spacing between the N-termini of the TMD helices in the dimer. We found two dimer
288 interfaces in TrkA-TMD that reside on opposite sides of the α-helix suggesting the
289 possibility of a rotation from one interface to the other upon NGF binding. If this model
290 were correct, mutual rotation of two motifs on the surface of the TM helix should activate
291 TrkA in the absence of NGF or increase its basal activation by overexpression. To test this
292 mechanism we introduced a different number of leucine residues into the TrkA-TMD and
293 analyzed the resulting TrkA activation in the absence of NGF (Figure 5B). The insertion of
294 each Leu should rotate the intracellular region around an angle of approximately 100º.
295 Thus, Leu insertion allows evaluation of whether a change in the rotation angle of the

296 intracellular domain plays any role in TrkA activation (Figure 5C). We transfected the
297 constructs TrkA-ins1L, TrkA-ins2L, TrkA-ins3L and TrkA-ins4L that included 1 to 4
298 inserted leucines respectively. The insertion of one Leu, TrkA-ins1Leu, significantly
299 increased both the constitutive activation of TrkA in transfected Hela cells compared to that
300 of transfected TrkA-wt (Figure 5D and 5E) and the differentiation of PC12nnr5 cells
301 compared to wt-transfected cells (Figure 5F) in a ligand-independent manner. Equal levels
302 of all constructs were expressed at the plasma membrane as determined using flow
303 cytometry (Figure S8). These data indicate that a rotation of the TMD is likely to underlie
304 TrkA activation.
305
306
307 **Discussion**
308 TrkA belongs to a subfamily of RTKs that includes the other family members TrkB and
309 TrkC. These RTKs are essential for the formation of the nervous system and mediate a
310 variety of cellular responses in normal biological processes and in pathological states (39).
311 An understanding of their mechanism of action is necessary to facilitate the design of new
312 pharmacological agents targeted to the processes in which they play a role.
313 Both TrkA and TrkB are in a pre-formed dimeric state in the absence of ligand and are
314 inactive in this state (18, 40). Using *in vivo* crosslinking and fluorescence complementation
315 assays in PC12 cells that express endogenous TrkA, Maruyama et al. found that TrkA, as
316 well as TrkB, form inactive dimers in the absence of NGF (18, 40). Marchetti et al., using
317 single-tracking of TrkA receptors, recently found that around 20% of plasma membrane-
318 expressed TrkA receptors are in a pre-dimer state in the absence of NGF (19). Additionally,
319 the existence of pre-formed dimers of full-length TrkA expressed in the plasma membrane
320 of Xenopus oocytes was shown by freeze-fracture electron microscopy (17). A recent study

321 has provided a further evidence for the existence of pre-formed dimers in the Trk family
322 (20). The laboratory of Dr. Hristova found that TrkA, as well TrkB and TrkC, exist in an
323 equilibrium monomer-dimer state in the absence of ligand depending on the expression
324 levels (20). That study also showed that the TMD and the intracellular domains of TrkA
325 contribute significantly to its unliganded dimerization. In the same work the authors
326 suggested that the equilibrium constant of TrkA dimerization indicated that endogenous
327 levels, for instance in PC12 cells, the most predominant form of TrkA is a monomer (80%)
328 in equilibrium with a 20% of pre-formed inactive dimers, supporting the data from
329 Marchetti et al. (19). Single-particle tracking showed that TrkA monomer form dimers and
330 oligomers upon NGF stimulation. Altogether TrkA activation follows a *transition* from a
331 monomer to a pre-former inactive dimer and to a full active ligand-bound dimer and
332 oligomers, in what has been called the "*transition model of RTK activation*" (20).
333 In this regard, in the present work we posed two major questions: (1) what are the
334 conformations of TrkA TMDs in the active/inactive states? and (2) how is the coupling
335 between the ligand binding and conformational switch accomplished? To answer the first
336 question we employed structural characterization using NMR spectroscopy together with
337 mutagenesis studies, disulfide cross-linking and functional assays. We described the high-
338 resolution NMR structure of the TrkA transmembrane domain dimer, which is the first such
339 description of a neurotrophin receptor of the Trk family. The obtained spatial structure was
340 verified using functional assays and cross-linking, which confirmed both the relevance of
341 this structure for TrkA activity and assignation of the found dimer conformation to the
342 receptor active state. This result, combined with the crystal structure of the extracellular
343 domain of the TrkA complex with NGF (16, 41), the crystal structure of the TrkA inactive
344 kinase domain (21, 22) and the recently reported structures of the entire TrkA intracellular

345 region (42, 43) provides an almost complete picture of the full length Trk receptor family,
346 lacking only the structure of the small JTM regions.
347 Additionally, we found another possible TMD dimerization interface using a genetic assay,
348 and functional tests indicated that this interface was also relevant for TrkA activation.
349 Although destruction of this interface by replacement of a small amino acid residue with a
350 bulky residue inhibited the dimerization in the bacterial membranes, it does not affect the
351 activation of TrkA by NGF, suggesting that this dimer interface is not populated in the full-
352 length TrkA receptor at least in the ligand-bound state. The structural data indicates that
353 this interface is an opposite side as the active dimer interface. Interestingly in an ideal α-
354 helix connected to the TMD the residues from the eJTM that form inactive dimers when
355 mutated to cysteine are located in the same helix side than the SxxxG motif. This suggests
356 that rotation of the eJTM will also rotate the TMD. Based on this it is possible that the
357 SxxxG interface forms part of an inactive pre-dimer state, although we cannot detect the
358 formation of dimers when the SxxxG motif is mutated to cysteine. One possibility is that, in
359 the inactive state, the distance between the SxxxG motifs are longer than the required for
360 the disulfide bond formation. This could be due to the presence of steric clashes from the
361 TrkA ICD or ECD, that are absent in the ToxRed constructs. However the finding that the
362 mutation of the G423I reduces significantly the differentiation of PC12 cells with NGF but
363 not the activation of the kinase domain (as shown by the phosphorylation of the Tyr-
364 674/675) is intriguing. PC12 cells differentiation needs of a sustained MAPK activation to
365 differentiate and it is plausible that a higher activation of TrkA is reached by the lateral
366 association of liganded dimers; i.e oligomerization of TrkA dimers. Actually the formation
367 of TrkA oligomers by NGF has been already described by single-particle tracking in
368 neuroblastoma cells (19). And oligomerization of ligand-bound RTKs seems a general
369 mechanism to regulate differential intracellular signalling (44). The important role of G423

370 in cell differentiation and its location in an opposite side of the α-helix to the active dimer
371 interface, suggests that G423 may participate in a protein-protein interface corresponding to
372 a supra-dimer (oligomer) form of the TrkA receptor that is populated upon NGF binding
373 (19). In this context further investigation on the TrkA oligomer formation is warranted.
374 To answer the second question posed above, we investigated the role of the eJTM regions
375 of the TrkA receptor upon NGF binding in receptor activation and dimerization. We
376 showed that full-length TrkA receptors can be activated by specific single-point mutations
377 in the eJTM, in which the position of the mutation relative to the TMD was more important
378 for activation than the dimerization propensity of the mutant.
379 Bearing all of these findings in mind, we propose a mechanism of receptor activation that is
380 outlined in Figure 6. In the model of the Figure 6, NGF binding to the Ig2 will induce a
381 rotation of the eJTM to facilitate the dimerization of the TMD via a preferred interface. This
382 model is supported by our data that showed that cysteine mutants in the eJTM in some
383 specific positions can activate TrkA without ligand and NGF binding brings the N-termini of
384 the α-helices into close proximity. The insertion of Leu residues downstream of the TMD
385 dimerization motif activated TrkA in the absence of ligand. This suggests that rotation of the
386 downstream domain may be behind the activation of the kinase domain. The rotational
387 mechanism of RTK activation has been proposed by other authors (45, 46). In this model the
388 ligand would induce a rotation of the TMD dimer interface that will re-orient the kinase
389 domains in order to facilitate the trans-phosphorylation. Although our results support this
390 model of activation other alternative possibilities may exist. For instance the insertion of
391 extra-residues increases the TMD length and could induce a piston-like mechanism of
392 activation by a pulling-down force. However an increase in the length by two, three or four
393 residues should also activate the kinase and this was not the case, as only the Ins1L mutant
394 showed activation. Also as the insertion of the residues are located into the TMD it may alter

395 the dimer interface of the TMD dimer leading to the formation of another dimer interface
396 compatible with a higher activation of the kinase domains. Although we cannot discard this
397 possibility, in the constructs we made the Leu residues are inserted upstream of the active
398 dimer interface in order to not alter the dimer interface found by NMR studies. In any case
399 the results obtained from the insertion mutagenesis suggest a conformational activation of
400 TrkA activation. Future structural and functional studies of the TrkA intracellular domain
401 should address how the kinase domain is activated if they are connected to the TMD by a
402 flexible intracellular juxtamembrane region.

403 In summary our data supports a conformational activation of TrkA by NGF and we have
404 provided functional and structural evidences of the roles played by the TMD in TrkA
405 dimerization and activation by NGF.

406

407 **References**

408 1. Chao, M. V., Neurotrophins and their receptors: a convergence point for many signalling
409 pathways. *Nat. Rev. Neurosci.* **2003,** *4* (4), 299-309.
410 2. Bothwell, M., NGF, BDNF, NT3, and NT4. *Handb. Exp. Pharmacol.* **2014,** *220*, 3-15.
411 3. Ceni, C.; Unsain, N.; Zeinieh, M. P.; Barker, P. A., Neurotrophins in the regulation of cellular
412 survival and death. *Handb. Exp. Pharmacol.* **2014,** *220*, 193-221.
413 4. Friedman, W. J.; Greene, L. A., Neurotrophin signaling via Trks and p75. *Exp. Cell Res.* **1999,**
414 *253* (1), 131-42.
415 5. Bothwell, M., Recent advances in understanding neurotrophin signaling. *F1000Res* **2016,** *5*.
416 6. Vilar, M., Structural Characterization of the p75 Neurotrophin Receptor: A Stranger in the
417 TNFR Superfamily. *Vitam Horm* **2017,** *104*, 57-87.
418 7. Smeyne, R. J.; Klein, R.; Schnapp, A.; Long, L. K.; Bryant, S.; Lewin, A.; Lira, S. A.;
419 Barbacid, M., Severe sensory and sympathetic neuropathies in mice carrying a disrupted Trk/NGF
420 receptor gene. *Nature* **1994,** *368* (6468), 246-9.
421 8. Indo, Y.; Tsuruta, M.; Hayashida, Y.; Karim, M. A.; Ohta, K.; Kawano, T.; Mitsubuchi, H.;
422 Tonoki, H.; Awaya, Y.; Matsuda, I., Mutations in the TRKA/NGF receptor gene in patients with
423 congenital insensitivity to pain with anhidrosis. *Nat. Genet.* **1996,** *13* (4), 485-8.
424 9. Martin-Zanca, D.; Hughes, S. H.; Barbacid, M., A human oncogene formed by the fusion of
425 truncated tropomyosin and protein tyrosine kinase sequences. *Nature* **1986,** *319* (6056), 743-8.
426 10. Cocco, E.; Scaltriti, M.; Drilon, A., NTRK fusion-positive cancers and TRK inhibitor therapy.
427 *Nat. Rev. Clin. Oncol.* **2018,** *15* (12), 731-747.

428 11. Endres, N. F.; Barros, T.; Cantor, A. J.; Kuriyan, J., Emerging concepts in the regulation of the
429 EGF receptor and other receptor tyrosine kinases. *Trends Biochem. Sci.* **2014,** *39* (10), 437-46.
430 12. Lemmon, M. A.; Schlessinger, J., Cell signaling by receptor tyrosine kinases. *Cell* **2010,** *141*
431 (7), 1117-34.
432 13. Wiesmann, C.; Ultsch, M. H.; Bass, S. H.; de Vos, A. M., Crystal structure of nerve growth
433 factor in complex with the ligand-binding domain of the TrkA receptor. *Nature* **1999,** *401* (6749), 184-
434 8.
435 14. Arevalo, J. C.; Conde, B.; Hempstead, B. I.; Chao, M. V.; Martin-Zanca, D.; Perez, P., A novel
436 mutation within the extracellular domain of TrkA causes constitutive receptor activation. *Oncogene*
437 **2001,** *20* (10), 1229-34.
438 15. Zaccaro, M. C.; Ivanisevic, L.; Perez, P.; Meakin, S. O.; Saragovi, H. U., p75 Co-receptors
439 regulate ligand-dependent and ligand-independent Trk receptor activation, in part by altering Trk
440 docking subdomains. *J. Biol. Chem.* **2001,** *276* (33), 31023-9.
441 16. Wehrman, T.; He, X.; Raab, B.; Dukipatti, A.; Blau, H.; Garcia, K. C., Structural and
442 mechanistic insights into nerve growth factor interactions with the TrkA and p75 receptors. *Neuron*
443 **2007,** *53* (1), 25-38.
444 17. Mischel, P. S.; Umbach, J. A.; Eskandari, S.; Smith, S. G.; Gundersen, C. B.; Zampighi, G. A.,
445 Nerve growth factor signals via preexisting TrkA receptor oligomers. *Biophys. J.* **2002,** *83* (2), 968-76.
446 18. Shen, J.; Maruyama, I. N., Nerve growth factor receptor TrkA exists as a preformed, yet
447 inactive, dimer in living cells. *FEBS Lett.* **2011,** *585* (2), 295-9.
448 19. Marchetti, L.; Callegari, A.; Luin, S.; Signore, G.; Viegi, A.; Beltram, F.; Cattaneo, A., Ligand
449 signature in the membrane dynamics of single TrkA receptor molecules. *J. Cell Sci.* **2013,** *126* (Pt 19),
450 4445-56.
451 20. Ahmed, F.; Hristova, K., Dimerization of the Trk receptors in the plasma membrane: effects of
452 their cognate ligands. *Biochem. J.* **2018,** *475* (22), 3669-3685.
453 21. Artim, S. C.; Mendrola, J. M.; Lemmon, M. A., Assessing the range of kinase autoinhibition
454 mechanisms in the insulin receptor family. *Biochem. J.* **2012,** *448* (2), 213-20.
455 22. Bertrand, T.; Kothe, M.; Liu, J.; Dupuy, A.; Rak, A.; Berne, P. F.; Davis, S.; Gladysheva, T.;
456 Valtre, C.; Crenne, J. Y.; Mathieu, M., The crystal structures of TrkA and TrkB suggest key regions for
457 achieving selective inhibition. *J. Mol. Biol.* **2012,** *423* (3), 439-53.
458 23. Bocharov, E. V.; Bragin, P. E.; Pavlov, K. V.; Bocharova, O. V.; Mineev, K. S.; Polyansky, A.
459 A.; Volynsky, P. E.; Efremov, R. G.; Arseniev, A. S., The Conformation of the Epidermal Growth
460 Factor Receptor Transmembrane Domain Dimer Dynamically Adapts to the Local Membrane
461 Environment. *Biochemistry* **2017,** *56* (12), 1697-1705.
462 24. Li, E.; Hristova, K., Role of receptor tyrosine kinase transmembrane domains in cell signaling
463 and human pathologies. *Biochemistry* **2006,** *45* (20), 6241-51.
464 25. Li, E.; Hristova, K., Receptor tyrosine kinase transmembrane domains: Function, dimer
465 structure and dimerization energetics. *Cell adhesion migration* **2010,** *4* (2), 249-54.
466 26. Jura, N.; Endres, N. F.; Engel, K.; Deindl, S.; Das, R.; Lamers, M. H.; Wemmer, D. E.; Zhang,
467 X.; Kuriyan, J., Mechanism for activation of the EGF receptor catalytic domain by the juxtamembrane
468 segment. *Cell* **2009,** *137* (7), 1293-307.
469 27. King, C.; Hristova, K., Direct measurements of VEGF:VEGFR2 binding affinities reveal the
470 coupling between ligand binding and receptor dimerization. *J. Biol. Chem.* **2019**.
471 28. Sarabipour, S.; Ballmer-Hofer, K.; Hristova, K., VEGFR-2 conformational switch in response
472 to ligand binding. *eLife* **2016,** *5*, e13876.
473 29. Sarabipour, S.; Hristova, K., Mechanism of FGF receptor dimerization and activation. *Nature*
474 *communications* **2016,** *7*, 10262.

475 30. Berger, B. W.; Kulp, D. W.; Span, L. M.; DeGrado, J. L.; Billings, P. C.; Senes, A.; Bennett, J.
476 S.; DeGrado, W. F., Consensus motif for integrin transmembrane helix association. *Proc. Natl. Acad.*
477 *Sci. U. S. A.* **2010,** *107* (2), 703-8.
478 31. Russ, W. P.; Engelman, D. M., TOXCAT: a measure of transmembrane helix association in a
479 biological membrane. *Proc. Natl. Acad. Sci. U. S. A.* **1999,** *96* (3), 863-8.
480 32. Nadezhdin, K. D.; Garcia-Carpio, I.; Goncharuk, S. A.; Mineev, K. S.; Arseniev, A. S.; Vilar,
481 M., Structural Basis of p75 Transmembrane Domain Dimerization. *J. Biol. Chem.* **2016,** *291* (23),
482 12346-57.
483 33. Mineev, K. S.; Lesovoy, D. M.; Usmanova, D. R.; Goncharuk, S. A.; Shulepko, M. A.;
484 Lyukmanova, E. N.; Kirpichnikov, M. P.; Bocharov, E. V.; Arseniev, A. S., NMR-based approach to
485 measure the free energy of transmembrane helix-helix interactions. *Biochim. Biophys. Acta* **2014,** *1838*
486 (1 Pt B), 164-72.
487 34. Mineev, K. S.; Goncharuk, S. A.; Arseniev, A. S., Toll-like receptor 3 transmembrane domain
488 is able to perform various homotypic interactions: an NMR structural study. *FEBS Lett.* **2014,** *588* (21),
489 3802-7.
490 35. Bocharov, E. V.; Mineev, K. S.; Goncharuk, M. V.; Arseniev, A. S., Structural and
491 thermodynamic insight into the process of "weak" dimerization of the ErbB4 transmembrane domain
492 by solution NMR. *Biochim Biophys Acta* **2012,** *1818* (9), 2158-70.
493 36. Cymer, F.; Veerappan, A.; Schneider, D., Transmembrane helix-helix interactions are
494 modulated by the sequence context and by lipid bilayer properties. *Biochim. Biophys. Acta* **2012,** *1818*
495 (4), 963-73.
496 37. Hughson, A. G.; Lee, G. F.; Hazelbauer, G. L., Analysis of protein structure in intact cells:
497 crosslinking in vivo between introduced cysteines in the transmembrane domain of a bacterial
498 chemoreceptor. *Protein Sci.* **1997,** *6* (2), 315-22.
499 38. Schecterson, L. C.; Hudson, M. P.; Ko, M.; Philippidou, P.; Akmentin, W.; Wiley, J.;
500 Rosenblum, E.; Chao, M. V.; Halegoua, S.; Bothwell, M., Trk activation in the secretory pathway
501 promotes Golgi fragmentation. *Mol. Cell. Neurosci.* **2010,** *43* (4), 403-13.
502 39. Deinhardt, K.; Chao, M. V., Trk receptors. *Handb. Exp. Pharmacol.* **2014,** *220*, 103-19.
503 40. Shen, J.; Maruyama, I. N., Brain-derived neurotrophic factor receptor TrkB exists as a
504 preformed dimer in living cells. *J Mol Signal* **2012,** *7* (1), 2.
505 41. Ultsch, M. H.; Wiesmann, C.; Simmons, L. C.; Henrich, J.; Yang, M.; Reilly, D.; Bass, S. H.;
506 de Vos, A. M., Crystal structures of the neurotrophin-binding domain of TrkA, TrkB and TrkC. *J. Mol.*
507 *Biol.* **1999,** *290* (1), 149-59.
508 42. Furuya, N.; Momose, T.; Katsuno, K.; Fushimi, N.; Muranaka, H.; Handa, C.; Ozawa, T.;
509 Kinoshita, T., The juxtamembrane region of TrkA kinase is critical for inhibitor selectivity. *Bioorg.*
510 *Med. Chem. Lett.* **2017,** *27* (5), 1233-1236.
511 43. Su, H. P.; Rickert, K.; Burlein, C.; Narayan, K.; Bukhtiyarova, M.; Hurzy, D. M.; Stump, C. A.;
512 Zhang, X.; Reid, J.; Krasowska-Zoladek, A.; Tummala, S.; Shipman, J. M.; Kornienko, M.; Lemaire, P.
513 A.; Krosky, D.; Heller, A.; Achab, A.; Chamberlin, C.; Saradjian, P.; Sauvagnat, B.; Yang, X.; Ziebell,
514 M. R.; Nickbarg, E.; Sanders, J. M.; Bilodeau, M. T.; Carroll, S. S.; Lumb, K. J.; Soisson, S. M.;
515 Henze, D. A.; Cooke, A. J., Structural characterization of nonactive site, TrkA-selective kinase
516 inhibitors. *Proc. Natl. Acad. Sci. U. S. A.* **2017,** *114* (3), E297-E306.
517 44. Needham, S. R.; Roberts, S. K.; Arkhipov, A.; Mysore, V. P.; Tynan, C. J.; Zanetti-Domingues,
518 L. C.; Kim, E. T.; Losasso, V.; Korovesis, D.; Hirsch, M.; Rolfe, D. J.; Clarke, D. T.; Winn, M. D.;
519 Lajevardipour, A.; Clayton, A. H.; Pike, L. J.; Perani, M.; Parker, P. J.; Shan, Y.; Shaw, D. E.; Martin-
520 Fernandez, M. L., EGFR oligomerization organizes kinase-active dimers into competent signalling
521 platforms. *Nature communications* **2016,** *7*, 13307.

522 45. Bell, C. A.; Tynan, J. A.; Hart, K. C.; Meyer, A. N.; Robertson, S. C.; Donoghue, D. J.,
523 Rotational coupling of the transmembrane and kinase domains of the Neu receptor tyrosine kinase. *Mol*
524 *Biol Cell* **2000,** *11* (10), 3589-99.
525 46. Maruyama, I. N., Activation of transmembrane cell-surface receptors via a common
526 mechanism? The "rotation model". *Bioessays* **2015,** *37* (9), 959-67.
527 47. Aoki, M.; Matsuda, T.; Tomo, Y.; Miyata, Y.; Inoue, M.; Kigawa, T.; Yokoyama, S.,
528 Automated system for high-throughput protein production using the dialysis cell-free method. *Protein*
529 *Expr. Purif.* **2009,** *68* (2), 128-36.
530 48. Kai, L.; Roos, C.; Haberstock, S.; Proverbio, D.; Ma, Y.; Junge, F.; Karbyshev, M.; Dotsch, V.;
531 Bernhard, F., Systems for the cell-free synthesis of proteins. *Methods Mol. Biol.* **2012,** *800*, 201-25.
532 49. Schwarz, D.; Junge, F.; Durst, F.; Frolich, N.; Schneider, B.; Reckel, S.; Sobhanifar, S.; Dotsch,
533 V.; Bernhard, F., Preparative scale expression of membrane proteins in Escherichia coli-based
534 continuous exchange cell-free systems. *Nat. Protoc.* **2007,** *2* (11), 2945-57.
535 50. Goncharuk, S. A.; Goncharuk, M. V.; Mayzel, M. L.; Lesovoy, D. M.; Chupin, V. V.;
536 Bocharov, E. V.; Arseniev, A. S.; Kirpichnikov, M. P., Bacterial Synthesis and Purification of Normal
537 and Mutant Forms of Human FGFR3 Transmembrane Segment. *Acta naturae* **2011,** *3* (3), 77-84.
538 51. Keller, R. L. J., The Computer Aided Resonance Assignment Tutorial. CANTINA Verlag:
539 Goldau, Switzerland, 2004.
540 52. Cavanagh, J., Fairbrother, W.J., Palmer, A.G. and Skelton, N.J., *Protein NMR spectroscopy:*
541 *principles and practice*. 2nd ed.; Academic Press,: San Diego, CA, USA, 2006.
542 53. Güntert, P., Automated NMR protein structure calculation. *Prog. NMR Spectrosc* **2003,** *43*, 105.
543 54. Shen, Y.; Bax, A., Protein backbone and sidechain torsion angles predicted from NMR
544 chemical shifts using artificial neural networks. *J. Biomol. NMR* **2013,** *56* (3), 227-41.
545 55. Koradi, R.; Billeter, M.; Wuthrich, K., MOLMOL: a program for display and analysis of
546 macromolecular structures. *J. Mol. Graph.* **1996,** *14* (1), 51-5, 29-32.
547 56. Polyansky, A. A.; Volynsky, P. E.; Efremov, R. G., Multistate organization of transmembrane
548 helical protein dimers governed by the host membrane. *J. Am. Chem. Soc.* **2012,** *134* (35), 14390-400.
549
550

551

552
553 **Material and Methods**

554 **DNA constructs**

555 A plasmid encoding rat TrkA with an N-terminal HA tag was kindly provided by Dr. Y
556 Barde. All TrkA mutants and constructs were derived from this plasmid. Mutagenesis was
557 done using the Site-directed mutagenesis kit (Agilent) according to the manufacturer's
558 protocol. The oligonucleotide sequences of all of the constructs are available upon request.
559 All DNA constructs were sequenced using local facilities.

560

561 **Cell culture and transfection**

562 Hela cells, which do not express endogenous TrkA, were cultured in DMEM medium
563 (Fisher) supplemented with 10% FBS (Fisher) at 37 °C in a humidified atmosphere with 5%
564 CO_2. PC12 and PC12nnr5 cells were cultured in DMEM with 10% FBS and 5% horse serum
565 (Fisher). Transfection of Hela cells was performed using polyethylenimine (PEI; Sigma) at a
566 concentration of 1-2 μg/μl. The use of PEI as the transfection reagent for Hela cells resulted
567 in suboptimal transfection (10-15% of cells transfected) and in the expression of only a small
568 amount of TrkA in the cells. In contrast, when the same PEI/DNA ratio was used for
569 transfection of Hek293 cells TrkA was expressed in higher amounts and ligand-independent
570 activation of TrkA was seen. A concentration of 500-1000 ng of DNA per 10 cm cell plate
571 was used for the TrkA activation experiments. Twenty four hours after transfection the cells
572 were lifted and re-plated into 12-well plates at a density of 100,000 cells per well. By using
573 this procedure the percentage of cells transfected was identical in all the wells. Forty eight
574 hours after transfection the cells were starved in serum free medium for 2 h and were then
575 stimulated with NGF (Alomone) at the indicated concentrations and time intervals. Cells
576 were lysed with TNE buffer (Tris-HCl pH 7.5, 150 mM NaCl, 1 mM EDTA) supplemented
577 with 1% triton X-100 (Sigma), protease inhibitors (Roche), 1 mM PMSF (Sigma), 1 mM
578 sodium orthovanadate (Sigma), and 1 mM sodium fluoride (Sigma). In the experiments
579 involving the TrkA cysteine mutants, 10 mM iodoacetamide (Sigma) was added to the lysis
580 buffer. Lysates were kept on ice for 10 minutes and centrifuged at 12,000 g for 15 minutes
581 in a tabletop centrifuge. The protein level of the lysates was quantified using a Bradford kit
582 (Pierce) and lysates were analyzed by SDS-PAGE

583

584 **Western blot analysis**

585 Cellular debris was removed by centrifugation at 12,000 g for 15 minutes and the protein
586 level of cell lysates was quantified using the Bradford assay (Pierce). Proteins were resolved
587 in SDS-PAGE gels and transferred to nitrocellulose membranes that were incubated
588 overnight at 4 ºC with one of the following antibodies: mouse monoclonal anti-HA (1:2000,
589 Sigma); rabbit polyclonal MBP-probe (1:1000, Santa Cruz); rabbit anti-phosphoTyr674/5
590 (1:1000, Cell Signaling); rabbit anti-TrkA (1:1000, Millipore). Following incubation with the
591 appropriate secondary antibody, membranes were imaged and bands quantified using
592 enhanced chemiluminescence and autoradiography.
593
594 **ToxRED assays**
595 Bacterial colonies were inoculated into LB medium (with 50 µg/ml ampicillin). Fresh LB
596 cultures (with 50 µg/ml ampicillin) were inoculated from fresh plates and were grown at 37
597 °C until they reached an O.D. of approximately 600≈0.6. They were then harvested by
598 centrifugation. Cells were subsequently lysed in lysis buffer (TNE, see recipe above) under
599 gentle conditions to avoid mCherry denaturation. After transfer to 1.5-mL Eppendorf tubes,
600 the mixture was incubated at room temperature with gentle agitation for 30 min. Samples
601 were then centrifuged for 10 min at 12000 × *g* to remove cell debris and to clarify the
602 supernatants for analysis. Aliquots (150 µl) of clarified supernatant were transferred to black,
603 opticlear 96-well plates and mCherry emission spectra were collected using a plate reader
604 (Tecan, Maennedorf, CH) with an excitation wavelength of 587 nm and emission
605 wavelengths of 610–650 nm. Subsequently, aliquots were transferred from black to clear 96-
606 well plates and the absorbance was measured from 450 to 750 nm. Measurements of
607 mCherry and of construct expression were performed from at least 10 different colonies and
608 were normalized for the relative expression level of each construct using western blotting
609 with the anti-MBP antibody. For western blots, samples were mixed with equal volumes of

610 2× SDS-PAGE sample buffer, heated to 95 °C for 10 min, separated on 10% (w/v)
611 polyacrylamide mini-gels, and were blotted onto nitrocellulose membranes that were probed
612 with anti-MBP antibody. To analyze disulfide bond formation bacterial colonies were lysed
613 using TNE plus 10 mM iodoacetamide and were analyzed using non-reducing SDS-PAGE.
614

615 **TrkA-TMD constructs for cell-free expression**

616 The gene encoding the transmembrane domain of the human TrkA-TM
617 (MK_{410}KDETPFGVSVAVGLAVFACLFLSTLLLVLNKAGRRNK_{447}) was amplified by PCR
618 from six chemically synthesized oligonucleotide templates (Evrogen, Russia) whose
619 sequences partially overlapped along its sequence. The PCR products were cloned into a
620 pGEMEX-1 vector by three-component ligation using the NdeI, AatII and BamHI restriction
621 sites.
622

623 **Cell-free gene expression.**

624 A bacterial S30 cell-free extract was prepared from a 10 L culture of the E. coli
625 Rosetta(DE3)pLysS strain according to a previously described protocol. The S30 cell extract
626 was stored in 500 μl aliquots at -80 °C. The continuous exchange mode of preparation using
627 a 12.5 kDa membrane was used in this study. Preparative-scale reactions (2-3 ml of reaction
628 mixture) were carried out in 50 mL tubes. Optimal reaction conditions such as Mg2+ and K+
629 concentrations, the ratio of the reaction mixture (RM) to the feeding mixture (FM) or the
630 DNA concentration were established using homemade reactors based on the Mini-CECF-
631 Reactor previously described (47, 48). The final reaction mixture was: a standard FM:RM
632 ratio of 8:1 and a cell-free reaction mixture containing 100 mM HEPES ⁄0.83 mM EDTA
633 with KOH added to achieve a pH of 8.0, 0.1 mg/mL Folinic acid, 20 mM acetyl phosphate,
634 1.2 mM ATP, 0.8 mM each of G/C/UTP, 2 mM 1,4-dithiothreitol, 0.05% sodium azide, 2%

635 PEG-8000, 20 mM magnesium acetate, 270 mM potassium acetate, 60 mM creatine
636 phosphate, 1 mM each of 20 amino acids or 0.25% of a 20 amino-acid mix (CIL, USA), 1
637 tablet / 50 mL of complete protease inhibitor (Roche, Switzerland), 0.5 mg/mL E.coli tRNA
638 (Roche, Switzerland), 0.25 mg/mL creatine kinase from rabbit muscle (Roche, Switzerland),
639 0.05 mg/mL T7 RNA polymerase prepared using a previously described protocol (49), 0.1
640 U/μL Ribolock (Fermentas), 0.02 μg/μL plasmid DNA, and 30% S30 cell-free extract. All
641 reagents were provided by Sigma unless otherwise specified. Plasmid DNA was purified
642 using a Promega MaxiPrep kit. Reactions were conducted overnight at 34 °C and in an
643 Innova 44R shaker (New Brunswick) set at 150 rpm.
644
645 **Protein purification.**
646 The cell-free reaction mixture was diluted three-times with buffer A (50 mM Tris pH 8.0 and
647 200 mM NaCl). After 10 minutes of incubation the mixture was centrifuged for 10 min at
648 18000 *g* at room temperature. The precipitate was washed consecutively with buffer A
649 containing 30 μg/ml RNAse A (Fermentas) and buffer B (50 mM Tris pH 8.0 and 100 mM
650 NaCl). The target protein was solubilized with 200 μl buffer B containing 1% lauryl
651 sarcosine. After each step the protein was centrifuged for 10 min at 18.000 *g* at room
652 temperature and aliquots of the supernatant were analyzed using 12,5% Tricine SDS-PAGE
653 (53). The clarified protein solution was applied onto a 10/300 Tricorn column prepacked
654 with Superdex 200 (GE Healthcare) and pre-equilibrated with buffer B containing 0.2%
655 lauryl sarcosine. Protein-containing fractions were combined and precipitated using the
656 TCA/acetone procedure (50).
657
658 **Preparation of NMR samples in a membrane mimetic media**

659 The so-called "isotopic-heterodimer" (1:1 mixture of unlabeled and $^{15}N/^{13}C$-labeled peptides)
660 samples were prepared corresponding to the TrkA-TMD construct in order to solve its
661 structure. The powder containing the peptides of both samples was first dissolved in a 1:1
662 trifluoroethanol–H_2O mixture with the addition of deuterated DPC (d_{38}, 98%, CIL) and
663 phosphate buffer, and was then kept for several minutes in an ultrasound bath and
664 lyophilized. Subsequently, the dried samples were dissolved in 350 µl of a 9:1 H_2O:D_2O
665 mixture. To attain a uniform micelle size and uniform distribution of the peptide throughout
666 the micelles, the samples were sonicated in an ultrasound bath for several minutes until the
667 solution was completely transparent. The TrkA-TMD concentration in the isotopic-
668 heterodimer sample was 1.9 mM, and other conditions were: LPR 50:1, pH 5.9, and 20 mM
669 phosphate buffer. Samples were placed in Shigemi NMR tubes with a glass plunger.
670 Selective-residue labeling was implemented to avoid peaks overlapping while processing the
671 NMR spectra.
672

673 **NMR spectroscopy and spatial structure calculation**

674 NMR spectra were acquired at 45 °C using 600 and 800 MHz AVANCE III spectrometers
675 (Bruker BioSpin, Germany) equipped with pulsed-field gradient triple-resonance cryoprobes.
676 1H, 13C, and 15N resonances of TrkA-TMD were assigned with CARA software (51) using
677 two- and three-dimensional heteronuclear experiments (52): $^{1}H/^{15}N$-HSQC, $^{1}H/^{15}N$-TROSY,
678 $^{1}H/^{13}C$-HSQC, $^{1}H/^{15}N$-HNHA, $^{1}H/^{13}C/^{15}N$-HNCA, $^{1}H/^{13}C/^{15}N$-HN(CO)CA, $^{1}H/^{13}C/^{15}N$-HNCO,
679 3D-HccH-TOCSY, ^{13}C- and ^{15}N-edited NOESY-HSQC (recorded on 600 and 800 MHz
680 spectrometers, respectively). Dimeric spatial structures were calculated with the CYANA
681 program (53) based on torsion angle restraints estimated from the chemical shift values
682 obtained with the standard protocol of the TALOS-N program (54) and with intra- and inter-
683 monomeric NOE distance restraints derived through analysis of the three-dimensional ^{15}N-

684 and ^{13}C-edited NOESY and ^{15}N,^{13}C-F1-filtered/F3-edited-NOESY spectra (52) acquired for
685 "isotopic-heterodimer" samples. MOLMOL software was used to calculate the contact areas
686 between the dimer subunits and to visualize the structures (55). Hydrophobic properties of
687 the α-helices in the TrkA-TMD dimers were calculated using the molecular hydrophobicity
688 potential (MHP) approach implemented in the PREDDIMER program (56).
689

690 **Isolation of Membrane fractions**

691 TrkA mutants were overexpressed in Hela cells by transfection using PEI (1mg/ml). 48
692 hours after transfection cells were resuspended in 1ml ice-cold homogenization buffer (250
693 mM sucrose, 1mM EDTA, 10 mM tris buffer pH 7,1 plus protease inhibitors) and broken by
694 sonication in two time intervals (30,30 s) with 50W and frequency at 30 MHz on ice. The
695 broken cell homogenate was centrifugated for 10 minutes at 500g at 4ºC to remove whole
696 cells and nuclei. To collect the membrane fraction the cleared supernatant was centrifuged at
697 100,000*g* at 4ºC for 1h in a Beckman Optima MAX ultracentrifuge with a TLA110 rotor
698 using polycarbonate thick wall centrifuge tubes (Beckman coulter ref. 362305). The
699 supernatant that contains soluble proteins was removed and the pellet-containing membranes
700 was resuspended in 1ml ice-cold homogenization buffer by sonication and re-centrifuged at
701 100,000*g*. The final pellet contains the membrane fraction used to the iodine oxidation
702 protocol.
703

704 **Iodine oxidation for crosslinking of TrkA mutants**

705 As cysteine residues are buried deep in the phospholipid bilayer, membranes were isolated
706 and I2 was used as the oxidation agent following as in (Schwem & Fillingame, 2006).
707 Membrane fractions were diluted in the homogenization buffer (250 mM sucrose, 1mM
708 EDTA, 10 mM Tris buffer pH 7,1 plus protease inhibitors). Protein content was quantified

709 using a Bardford kit (Pierce) and equal amounts of isolated membranes fractions were
710 incubated for 10 min with or without NGF (10 ng/mL). A solution of 2.5 mM I2 in absolute
711 ethanol was freshly prepared immediately before the crosslinking of cysteine residues and
712 was added to the incubated membrane fractions with NGF (250 mM final Iodine
713 concentration) for 30 seconds at room temperature. The reaction was stop adding 1/10
714 volume of a freshly made solution of sodium thiosulfate (60 mM final concentration). Non-
715 reducing SDS-PAGE sample buffer was added and the samples were boiled for 5 minutes
716 before analyzed by non-reducing SDS-PAGE.
717
718 **Differentiation of PC12nnr5 cells.**
719 Transfection in PC12nnr5 cells was performed using Lipofectamine 2000 as per
720 manufacturer instructions. The mutant or the wild-type TrkA-transfected cells and mock-
721 transfected cells as well as non-transfected cells were treated under the same conditions in a
722 six-well tissue culture plate. The cells were washed three times with serum-free medium and
723 incubated for 48 h in a medium containing 1% fetal bovine serum and 50 ng/mL of NGF
724 (Alomone). At time 0, 24h and 48h, cells were washed with cold PBS and fixed with 4%
725 paraformaldehyde during 15 minutes at room temperature. Cells were imaged using a Leica
726 SP8 spectral confocal microscope. The percentage of cells with a neurite twice longer as the
727 cell body was counted as differentiated.
728
729
730 **Accession codes**
731 Atomic coordinates and experimental restraints were deposited in the Protein Data Bank
732 under the accession codes PDB ID: 2n90 for TrkA-TM-wt.
733

Acknowledgments

We thank Dr. Carlos Ibañez for critical reading of the manuscript, Dr. W. DeGrado for providing ToxRed plasmids, and Dr. Yves Barde for the TrkA plasmid. This study was supported by the Spanish Ministry of Economy and Competitiveness (MINECO; project BFU2013-42746-P and SAF2017-84096-R) and by the Generalitat Valenciana Prometeo Grant 2018/055 to MV). Studies of TrkA-TM homodimerization were supported by the Russian Science Foundation (grant No# 19-74-30014 to A.S.A).

Author Contributions

M.L.F. constructed the TrkA mutants and performed the TrkA activation, differentiation, functional and crosslinking experiments. K.D.N. designed and performed NMR experiments and analyzed NMR data. S.A.G. developed the expression protocols and synthesized samples for NMR analysis. K.S.M. analyzed NMR data and contributed to the preparation of the manuscript. A.S.A. and M.V. designed and supervised the entire project and wrote the manuscript.

759 **Figure Legends**

760 **Figure 1. Analysis of the structure of TrkA transmembrane domain dimers in the**
761 **ToxRED system and in DPC micelles**.

762 A) ToxRed system analysis and quantification of the percentage of dimerization of the rat
763 TrkA-TMD normalized to glycophorin A (GpA) wt (100%). GpA-wt* refers to an inactive
764 ToxR that cannot induce the RedFP.

765 B) Percentage of dimerization of rat TrkA-wt and TrkA-TMD mutants normalized to
766 dimerization of GpA wt (100%) in the ToxRed system. (In A and B results represent the
767 average of at least 10 colonies analyzed per experiment. Plotted is the result of at least
768 seven independent experiments). Error bars represent the standard error calculated from the
769 seven independent measurements. Statistics were performed using two-way ANOVA
770 analysis and Dunnet's multiple comparison test using GraphPad software. P values of
771 conditions significantly different from wt are shown on top of the error bars (****
772 $P<0.0001$).

773 C) Schematic representation of the NMR spatial structure of the human TrkA-TMD dimer
774 in lipid micelles, from different angles. The surface of one TMD helix is represented with
775 the $S_{419}xxxG_{423}$ motif in blue and the NMR dimer interface in red. The TMD of the other
776 monomer within the dimer is represented as ribbons, and side chains are indicated as sticks.
777 The location of the NMR dimer interface LxxFAxxF on the NMR structure is colored red
778 and other mutated residues are colored orange. The PDB accession code is 2n90.

779 D) Alignment of the amino acid sequences of the transmembrane helical domain of TrkA
780 from different species (h, homo sapiens, r, ratus norvegicus, m, mus musculus; c Gallus
781 gallus; z Danio rerio; x Xenopus laevis). The residues participating in the NMR dimer
782 interface are highlighted in red, and residues participating in dimerization based on the
783 ToxRED analysis are highlighted in blue.

784

785 **Figure 2. Functional identification of the two dimer interfaces in the TrkA-TMD**

786 A) Amino acid sequence of the transmembrane domain of rat TrkA showing the location of
787 the single cysteine residue substitutions.

788 B) Western blot of Hela cells transfected with the indicated TrkA-TMD constructs and
789 analyzed using non-reducing SDS PAGE, showing the formation of covalent cysteine
790 dimers (d) arising from monomers (m) crosslinked using molecular iodine (I_2) in the
791 presence or absence of NGF.

792 C) Quantification of the data in B) derived from at least three independent experiments.
793 Bars represent standard error of the mean. Statistics were performed using two-way
794 ANOVA analysis and Dunnet's multiple comparison test using GraphPad software. (****
795 P<0.0001, *** P=0.0004).

796 D) Structure of the TrkA-TMD dimer showing the location of the indicated residues in red.

797 E) Cβ-Cβ distance between the indicated residues in the TrkA-TMD.

798 F) Hela cells transfected with the indicated TrkA constructs were stimulated with NGF (10
799 ng/mL) for 0, 5 or 15 minutes. The immunoblots show the activation (autophosphorylation)
800 of TrkA as detected using an antibody specific for TrkA P-Tyr674/675. The levels of total
801 TrkA are shown below each blot. Molecular weight markers are shown at left.

802 G) Quantification of the data in F) derived from at least three independent experiments.
803 Bars represent standard error of the mean. Statistics were performed using two-way
804 ANOVA analysis and Dunnet's multiple comparison test using GraphPad software. P
805 values of conditions significantly different from wild type are shown on top of the error
806 bars.

807 H) Cytometric analysis of the expression of the TrkA mutants at the plasma membrane
808 (orange bars) and quantification of the percentage of PC12nnr5 differentiated cells (colored

809 bars) transfected with the indicated TrkA constructs together with GFP. EV, empty vector.
810 The percentage of the total GFP-positive transfected cells with a neurite twice as long as
811 the length of the cell body was quantified. Bars represent the standard error of at least three
812 independent experiments. Statistical analysis was performed using ordinary one-way
813 ANOVA, using Bonferroni's multicomparison test compared to wt. The P values of
814 significant differences are shown. ns, not significant.
815
816 **Figure 3. K410 and K411 of eJTM are crosslinked with BS3 upon NGF binding.**
817 A) Location of the Lys residues in the crystal structure of the rat TrkA-ECD/NGF complex
818 (PDB: 2IFG) (Wehrman et al., 2007). The Lys residues are shown as green circles are
819 located in the extracellular juxtamembrane region of the TrkA-ECD (in gray).
820 B) Western immunoblots of lysates of Hek293 cells transfected with the indicated TrkA
821 constructs (see Figure 3A) and incubated with or without NGF in the presence the cross
822 linker BS3. Molecular weights are indicated at left. Actin was assayed as a loading control.
823
824 **Figure 4. A preferred dimer interface in the TrkA juxtamembrane region.**
825 A) Amino acid sequence of the rat TrkA cysteine mutant constructs that are mutated in the
826 region of the eJTM closest to the TMD. B) Quantification of the ratio of dimer:monomer of
827 the TrkA mutants as determined using non-reducing SDS-PAGE. C) Quantification of the
828 activation of TrkA (with and without NGF) by quantifying the signal from the
829 phosphorylation of the Tyr 674/675 signal using western blotting of the cysteine mutants in
830 the JTM region. D) Scatter plot of the dimerization of TrkA cysteine mutants respect to its
831 activation in the absence of NGF. A regression fit using the active (green) and inactive
832 (red) cysteine mutant dimers is shown with the indicated r^2. E) PC12nnr5 cell
833 differentiation assay of TrkA-wt and TrkA-K410C in the presence and absence of NGF. E)

834 Quantification of the differentiation of PC12nnr5 cells transfected with the indicated TrkA
835 constructs and incubated in the absence (blue bars) or presence (green bars) of NGF. G)
836 Cytometric analysis of the expression of the TrkA mutants at the plasma membrane of Hela
837 cells. H) Model of the eJTM into an ideal α-helix showing the spacial location of the
838 indicted residues. Error bars represent the standard error of the mean. Statistics was done
839 using two-way ANOVA analysis and Dunnet's multiple comparison test using GraphPad
840 software. The P values of significant differences are shown (**** P<0.0001).
841
842 **Figure 5. Rotation of the TrkA-TMD as a mechanism of TrkA activation by NGF.**
843 A) Effect of NGF on the activation of overexpressed TrkA. Hela cells transfected with the
844 indicated constructs were stimulated with NGF (10 ng/mL) for 0, 5, 15 or 30 minutes. The
845 immunoblots show the activation of TrkA as detected using an antibody specific for the
846 autophosphorylated P-Tyr674/675, P-Tyr490 and P-Tyr751 residues and for the
847 downstream activated P-ERK. The levels of total TrkA and total ERK are shown below
848 each blot. Actin was blotted as a loading control. A representative blot of at least three
849 independent experiments is shown.
850 B) Amino acid sequences of the rat TrkA Leu insertion mutants indicating the location of
851 the inserted Leu residues.
852 C) Schematic drawing of the TrkA-TMD-ICD showing how the different numbers of
853 inserted Leu residues (blue) in the TMD induce a different rotation of the intracellular
854 domain (green).
855 D) Hela cells were transfected with the indicated TrkA-TMD insertion mutants. The
856 immunoblots show the activation of TrkA as detected using an antibody specific for the
857 TrkA autophosphorylation P-Tyr674/675 residues. The levels of total TrkA are shown
858 below. Actin was assayed as a loading control.

859 E) Quantification of the data in D) from at least three independent experiments. Bars
860 represent standard error of the mean. Statistical analysis was performed using one-way
861 ANOVA with Dunnet's multicomparison test and TrkA-wt as a control. The P value of the
862 significant difference is shown.
863 F) PC12nnr5 cell differentiation of TrkA-TMD insertion mutant-transfected cells incubated
864 in the absence of NGF. The percentage of the total GFP positive-transfected cells with a
865 neurite twice as long as the length of the cell body was quantified. Bars represent the
866 standard error of at least four independent experiments. Statistical analysis was performed
867 using one-way ANOVA with Dunnet's multicomparison test and TrkA-wt as a control. The
868 P values of significant differences are shown.
869
870 **Figure 6. Model of TrkA activation by NGF.**
871 TrkA exists in an equilibrium between a monomer and an inactive pre-dimer, which is
872 stabilized by interactions between Ig2 domains and between the inactive kinase domains.
873 Upon NGF binding a rotation of the Ig2 domain induces the formation of a crossed TMD
874 dimer that is stabilized by the protein interface determined in the NMR and functional
875 studies. The rotation of the TMD is transmitted to the intracellular region in order to
876 activate TrkA kinase autophosphorylation.

Figure 1- Table supplement 1

NMR distance & dihedral restraints	
Total unambiguous NOE restraints	360
intra-residue	136
inter-residue	228
sequential (|i-j|=1)	138
medium-range (1<|i-j|≤4)	76
long-range (|i-j|>4)	0
inter-monomeric NOE	16
Hydrogen bond restraints (upper/lower)	144/144
Total torsion angle restraints	118
backbone φ	52
backbone ψ	51
side-chain χ^1	15
Structure calculation statistics	
CYANA target function (Å^2)	0.64±0.21
Average pairwise r.m.s.d. (Å)	
TM α-helical region	
backbone atoms	0.18±0.07
all heavy atoms	0.36±0.07
Ramachandran analysis [a]	
% residues in most favoured regions	90.6
% residues in additional allowed regions	9.4
% residues in generously allowed regions	0.0
% residues in disallowed regions	0.0
Helix-helix packing	
Contact surface area per dimer subunit (Å^2)	370±40
Angle θ between the helix axes (deg.)	40±5
Distance d between the helix axes (Å)	
TM region	8.8±0.5

Table note:
[a] Ramachandran statistics was determined using CYANA
[b] Residues from unfolded and flexible regions

Figure 1

A

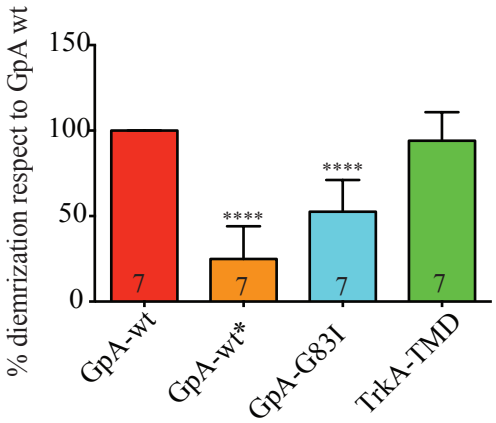

C

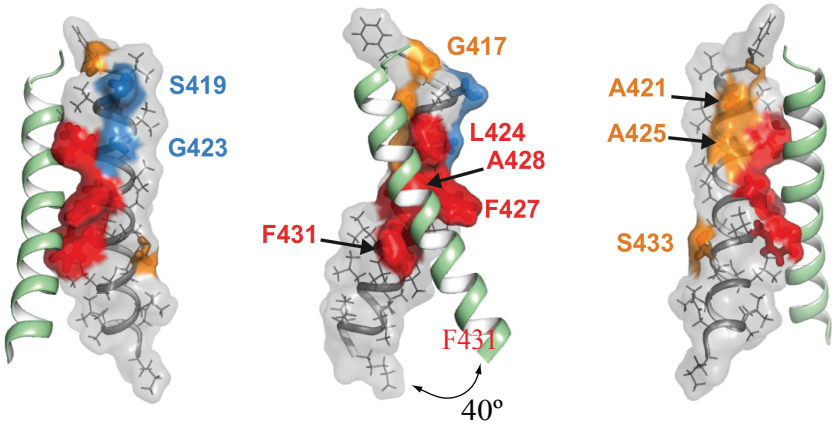

B

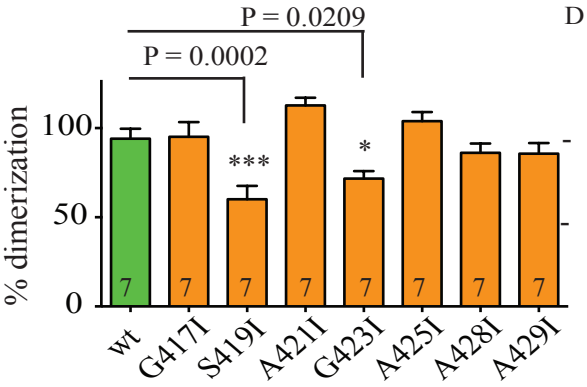

D

TM helix

```
hTrkA   TPFGVSVAVGLAVFACLFLSTLLLVL
rTrkA   TPFGVSVAVGLAVSAALFLSALLLVL
mTrkA   TPFGVSVAVGLAVSAALFLSALLLVL
cTrkA   HTFGVSVAVALAVFASLFLSVMLIAL
xTrkA   NTFGVSVAVGLAVFACLFLLLMLIAL
zTrkA   RVFGVSVAVGLAVFACTFLLIMVVVI

hTrkC   DTFGVSIAVGLAAFACVLLVVLFVMI
hTrkB   EHLSVYAVVVIASVVGFCLLVMLFLL
```

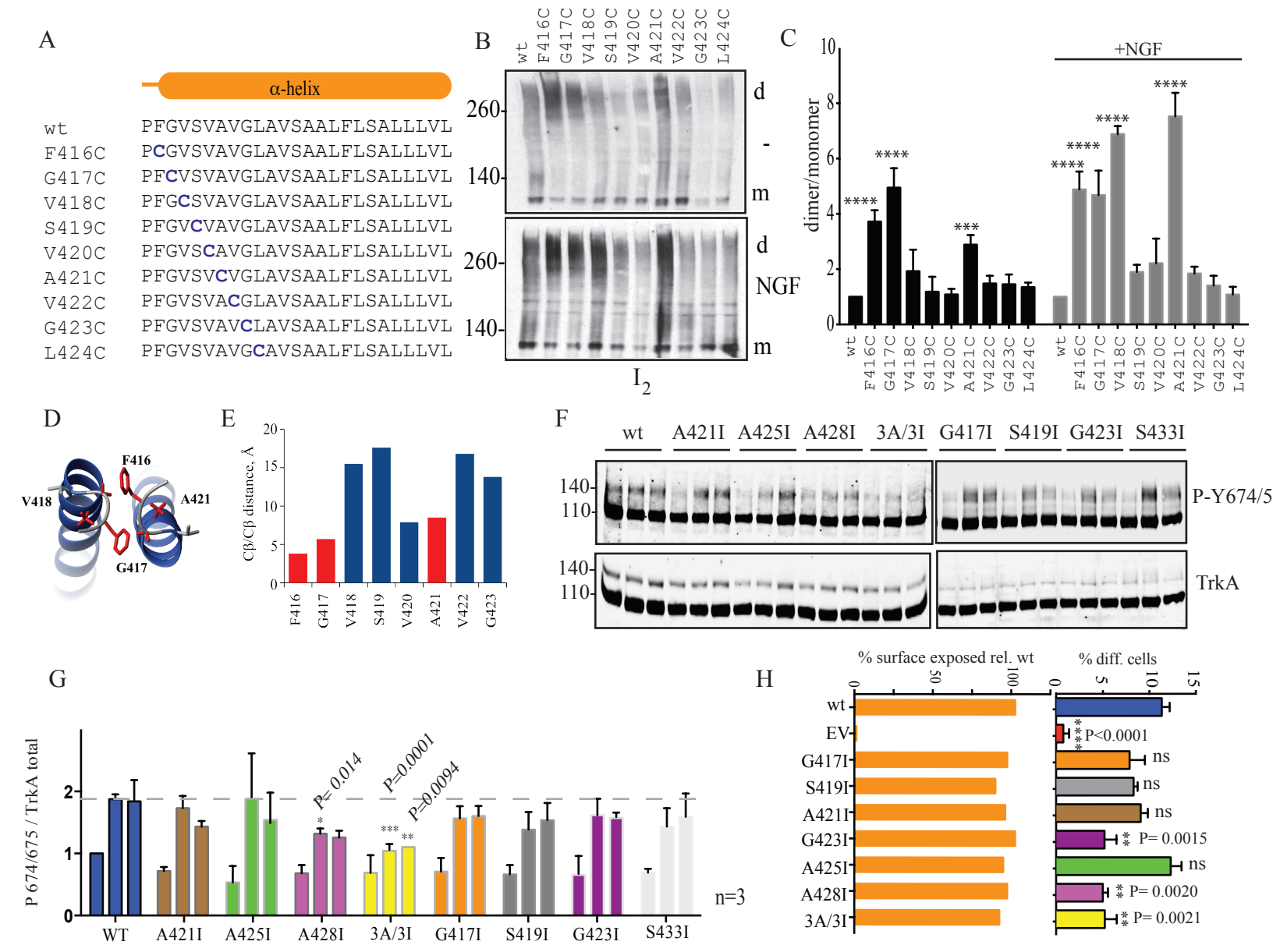
A
α-helix
wt PFGVSVAVGLAVSAALFLSALLLVL
F416C PCGVSVAVGLAVSAALFLSALLLVL
G417C PFCVSVAVGLAVSAALFLSALLLVL
V418C PFGCSVAVGLAVSAALFLSALLLVL
S419C PFGVCVAVGLAVSAALFLSALLLVL
V420C PFGVSCAVGLAVSAALFLSALLLVL
A421C PFGVSVCVGLAVSAALFLSALLLVL
V422C PFGVSVACGLAVSAALFLSALLLVL
G423C PFGVSVAVCLAVSAALFLSALLLVL
L424C PFGVSVAVGCAVSAALFLSALLLVL
B
wt F416C G417C V418C S419C V420C A421C V422C G423C L424C
260
140
d
-
m
NGF
I2
C
+NGF
dimer/monomer
D
F416
V418
A421
G417
E
Cβ/Cβ distance, Å
F416 G417 V418 S419 V420 A421 V422 G423
F
wt A421I A425I A428I 3A/3I G417I S419I G423I S433I
P-Y674/5
TrkA
G
P 674/675 / TrkA total
P= 0.014
P=0.0001
P=0.0094
WT A421I A425I A428I 3A/3I G417I S419I G423I S433I
n=3
H
% surface exposed rel. wt
% diff. cells
wt
EV
G417I
S419I
A421I
G423I
A425I
A428I
3A/3I
P<0.0001
ns
P= 0.0015
P= 0.0020
P= 0.0021

Figure 3

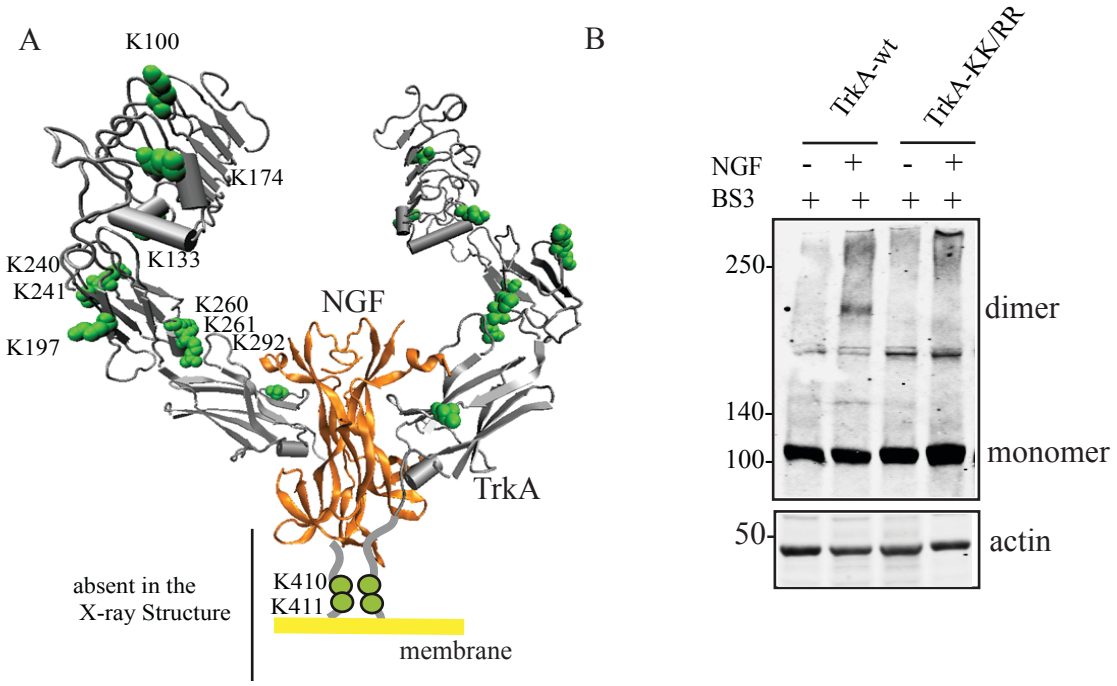
A
K100
K174
K133
K240
K241
K260
K261
K292
K197
NGF
TrkA
absent in the
X-ray Structure
K410
K411
membrane
B
TrkA-wt
TrkA-KK/RR
NGF
BS3
250
140
100
50
dimer
monomer
actin

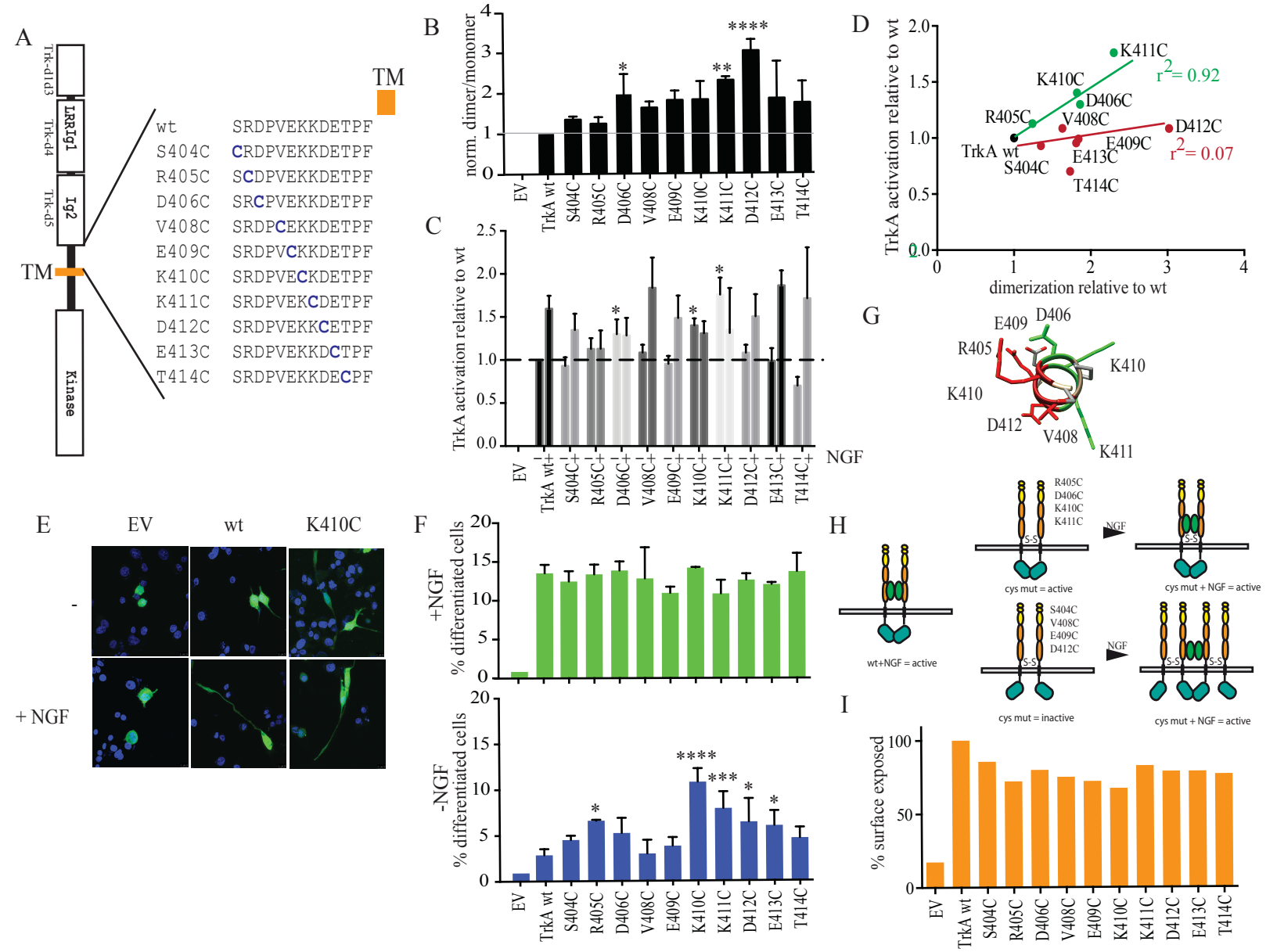
A
Trk-d1d3
LRRig1
Trk-d4
Ig2
Trk-d5
TM
Kinase
TM
wt SRDPVEKKDETPF
S404C CRDPVEKKDETPF
R405C SCDPVEKKDETPF
D406C SRCPVEKKDETPF
V408C SRDPCEKKDETPF
E409C SRDPVCKKDETPF
K410C SRDPVECKDETPF
K411C SRDPVEKCDETPF
D412C SRDPVEKKCETPF
E413C SRDPVEKKDCTPF
T414C SRDPVEKKDECPF
B
norm. dimer/monomer
EV
TrkA wt
S404C
R405C
D406C
V408C
E409C
K410C
K411C
D412C
E413C
T414C
C
TrkA activation relative to wt
NGF
D
TrkA activation relative to wt
dimerization relative to wt
K411C
K410C
D406C
R405C
V408C
D412C
E409C
TrkA wt
S404C
E413C
T414C
r2= 0.92
r2= 0.07
G
E409
D406
R405
K410
K410
D412
V408
K411
E
EV
wt
K410C
-
+ NGF
F
+NGF
% differentiated cells
-NGF
% differentiated cells
H
R405C
D406C
K410C
K411C
S-S
NGF
cys mut = active
cys mut + NGF = active
wt+NGF = active
S404C
V408C
E409C
D412C
cys mut = inactive
cys mut + NGF = active
I
% surface exposed

Figure 5

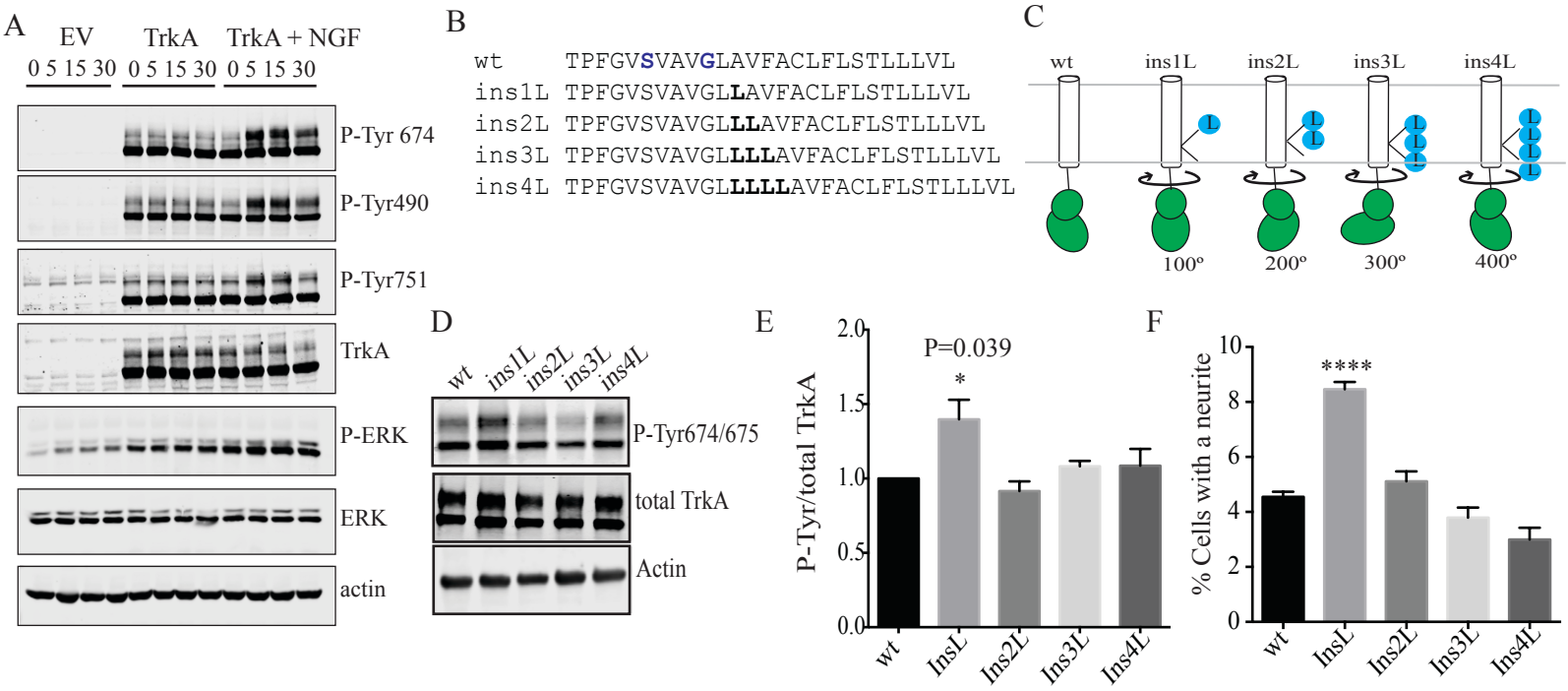
A
EV
TrkA
TrkA + NGF
0 5 15 30 0 5 15 30 0 5 15 30
P-Tyr 674
P-Tyr490
P-Tyr751
TrkA
P-ERK
ERK
actin
B
wt TPFGVSVAVGLAVFACLFLSTLLLVL
ins1L TPFGVSVAVGLLAVFACLFLSTLLLVL
ins2L TPFGVSVAVGLLLAVFACLFLSTLLLVL
ins3L TPFGVSVAVGLLLLAVFACLFLSTLLLVL
ins4L TPFGVSVAVGLLLLLAVFACLFLSTLLLVL
C
wt
ins1L
ins2L
ins3L
ins4L
100º
200º
300º
400º
D
wt
ins1L
ins2L
ins3L
ins4L
P-Tyr674/675
total TrkA
Actin
E
P-Tyr/total TrkA
P=0.039
*
2.0
1.5
1.0
0.5
0.0
wt
InsL
Ins2L
Ins3L
Ins4L
F
% Cells with a neurite
****
10
8
6
4
2
0
wt
InsL
Ins2L
Ins3L
Ins4L

Figure 6

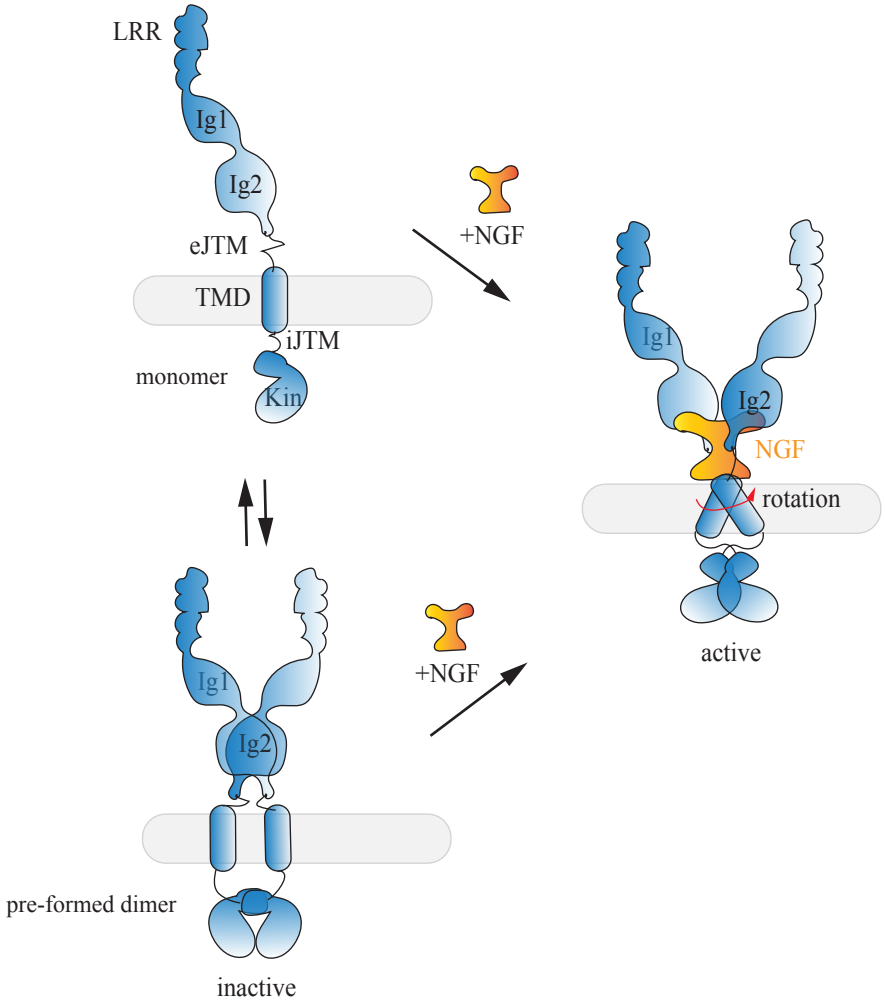
LRR
Ig1
Ig2
eJTM
TMD
iJTM
monomer
Kin
+NGF
Ig1
Ig2
NGF
rotation
active
Ig1
Ig2
+NGF
pre-formed dimer
inactive

Figure S1. Dimerization of the TrkA-TMD in micelles.

(A) Percentage of the monomeric (green), dimeric (blue) and oligomeric (red) forms of the human TrkA-TMD at different LPRs. Population values were calculated from the cross-peak intensities in the $^{1}H/^{15}N$-TROSY spectra.

(B) Apparent free energy of dimerization of the TrkA-TMD (ΔGapp) = RTln([M]2/[D]) plotted as a function of RTln(X), where X = ([Det]−Nm[M]−Nd[D])/Ne. [M], [D] and [Det] represent monomer, dimer and DPC concentration, respectively. Ne represents the number of DPC molecules per empty micelle, and Nm and Nd represent the number of DPC molecules per micelle for monomers and dimers, respectively.

Figure S2. The $^{1}H/^{15}N$-HSQC spectrum of the human TrkA-TMD-wt.

The human TrkA-TMD was solubilized in an aqueous suspension of DPC micelles at an LPR of 50:1, and at 45 °C and pH 5.9. $^{1}H–^{15}N$ backbone and side-chain resonance assignments are shown.

Figure S3. Summary of the NMR data for the TrkA-TMD embedded into DPC micelles.

A) NOE connectivities observed in the $^{1}H/^{15}N$-NOESY-HSQC spectrum for the TrkA-TM peptide.

B) Secondary $^{13}C\alpha$ chemical shifts of the TrkA-TMD are given by the difference between the actual chemical shift and a typical random-coil chemical shift for a specific residue. Pronounced positive or negative $\Delta\delta(^{13}C\alpha)_{h-c}$ values indicate a helical structure or an extended conformation of a protein.

Figure S4. Assessment of the quality of the NMR-derived TrkA-TMD dimer structure.

Structural alignment of the 10 lowest energy NMR structures of TrkA-TMD dimers.

Figure S5. **Hydrophobicity map of the TrkA-TMD dimer.**

The black oval delineates an helix-packing interface as calculated with the PREDIMER software. The residues within this black oval comprise the TrkA-TMD dimerization interface. The panels to the right show the percentage of inter-monomer contact surface area.

Figure S6. **TrkA-concentration-dependence of ligand-independent activation of TrkA**. Increasing amounts of TrkA were transfected into Hela cells using PEI. After 48 h, the cells were stimulated or not with NGF (10 ng/mL). Cell lysates were analyzed by SDS-PAGE immnoblotting using antibodies specific for TrkA phospho-Tyr674/675 and total TrkA.

Figure S7. Membrane localization of TrkA mutants in Hela cells. Confocal fluorescence images of Hela cells transiently transfected with the indicated TrkA constructs. The cells were fixed and analyzed using an antibody against HA located in the N-terminus of TrkA, which was detected with a secondary antibody conjugated with the fluorophore alexa-555 (Red). Blue, nuclear DAPI staining. The cells shown are representative of 10 transfected cells analyzed for each condition**.**

Figure S8. Membrane localization of TrkA mutants in Hela cells by cytometric analysis. Percentage of TrkA constructs expressed at the plasma membrane relative to TrkA-wt (100%) obtained in Hela cells transfected with the indicated constructs and

analyzed by flow cytometry using an HA primary antibody and a secondary antibody labeled with a fluorephore for alexa-488. EV is empty vector.

Figure S1

A

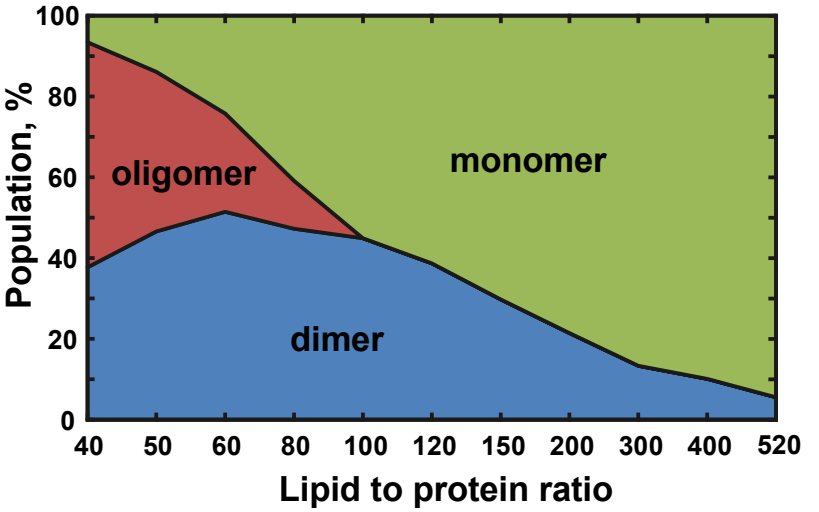
100
80
60
40
20
0
Population, %
oligomer
monomer
dimer
40
50
60
80
100
120
150
200
300
400
520
Lipid to protein ratio

B

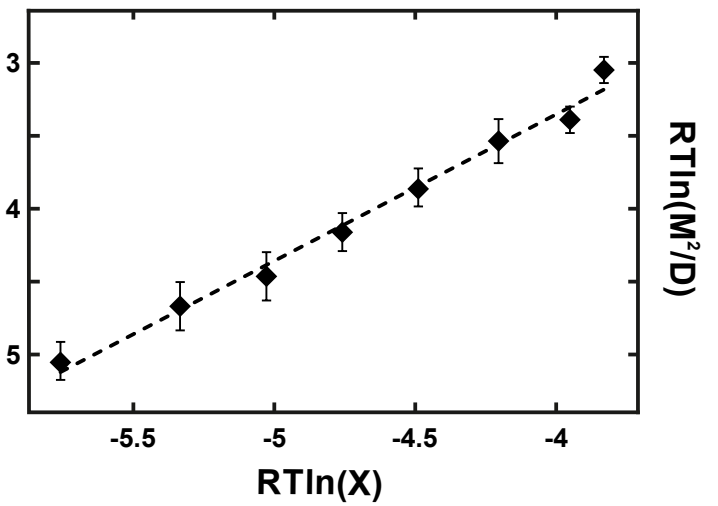
3
4
5
-5.5
-5
-4.5
-4
RTln(X)
RTln(M²/D)

Figure S2

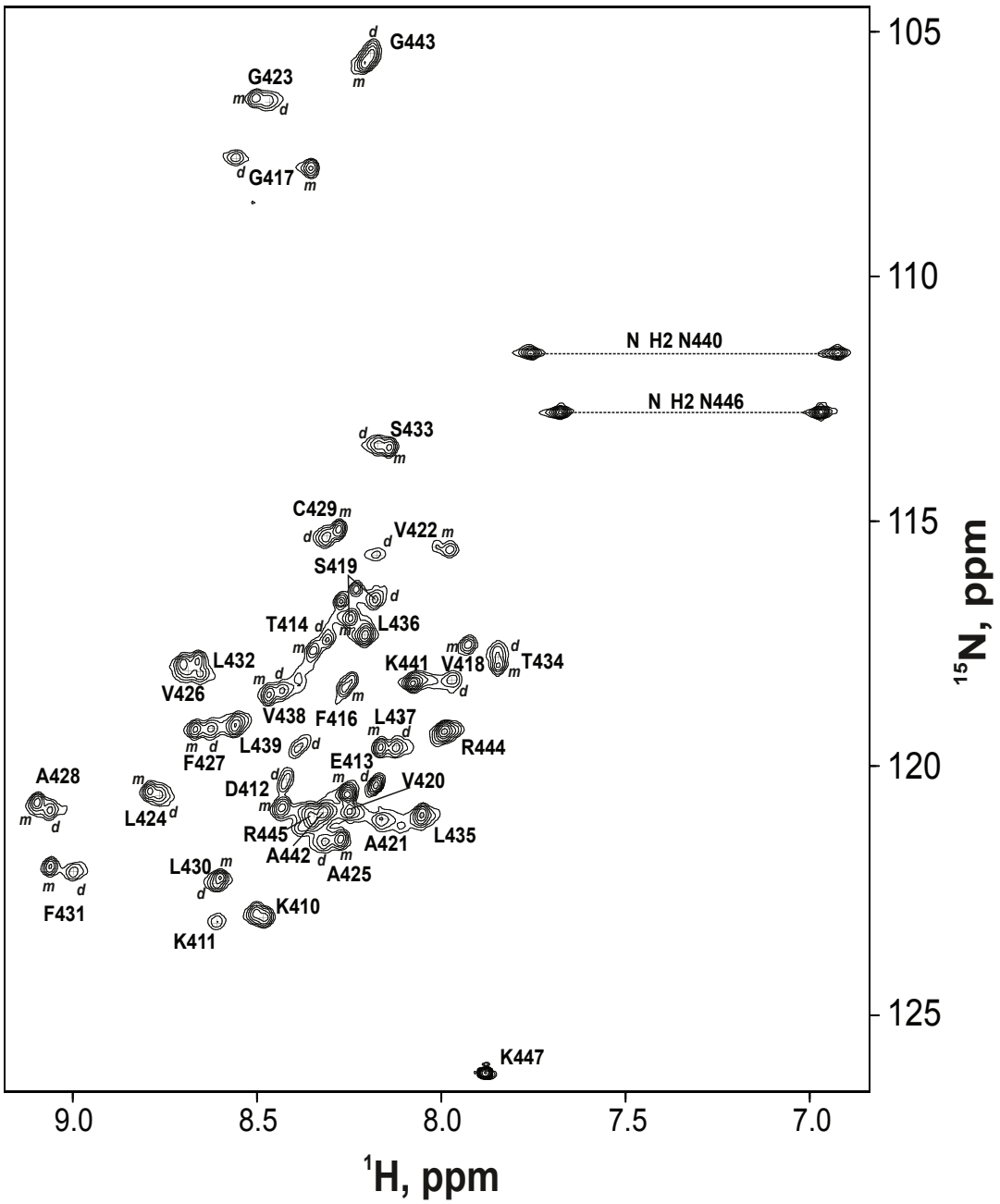
G443
G423
G417
N H2 N440
N H2 N446
S433
C429
V422
S419
T414
L436
L432
K441
V418
T434
V426
V438
F416
L437
L439
R444
F427
E413
A428
D412
V420
L424
R445
A421
L435
A442
A425
L430
F431
K410
K411
K447
105
110
115
120
125
9.0
8.5
8.0
7.5
7.0
^{15}N, ppm
^{1}H, ppm

Figure S3

A

B

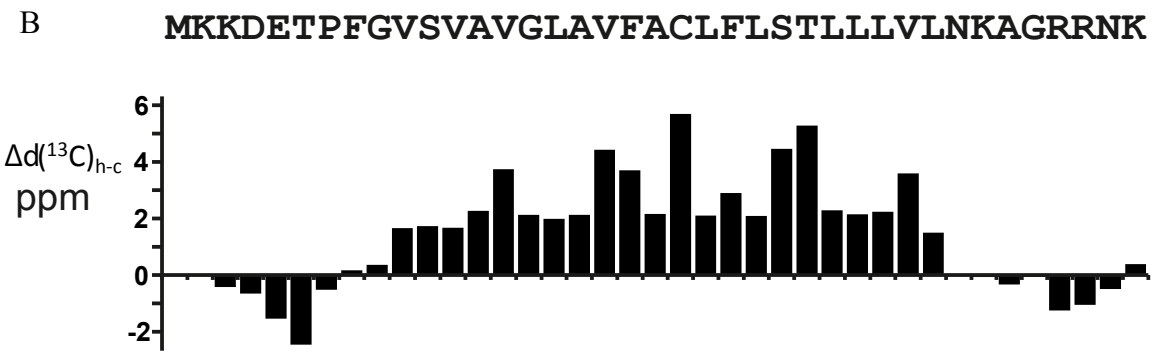

C

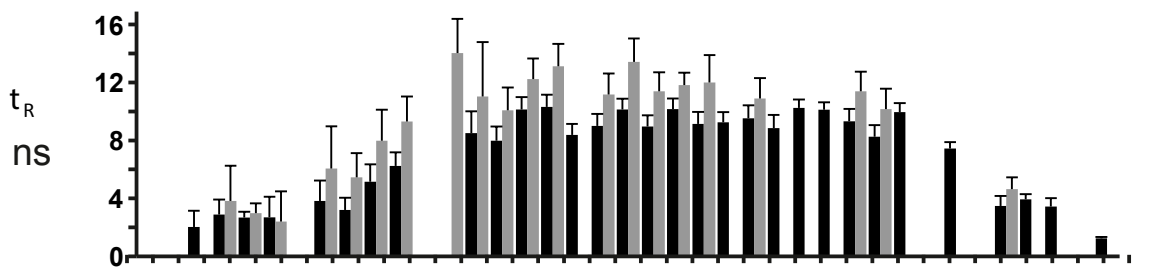

Figure S4

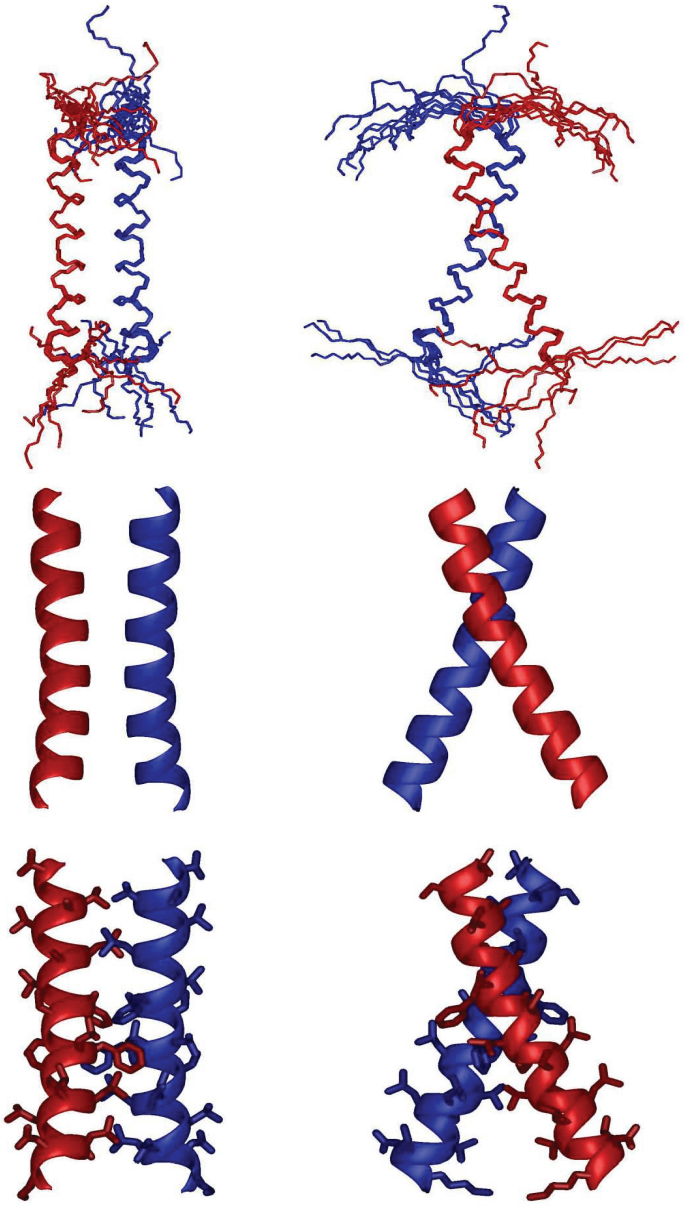

Figure S5

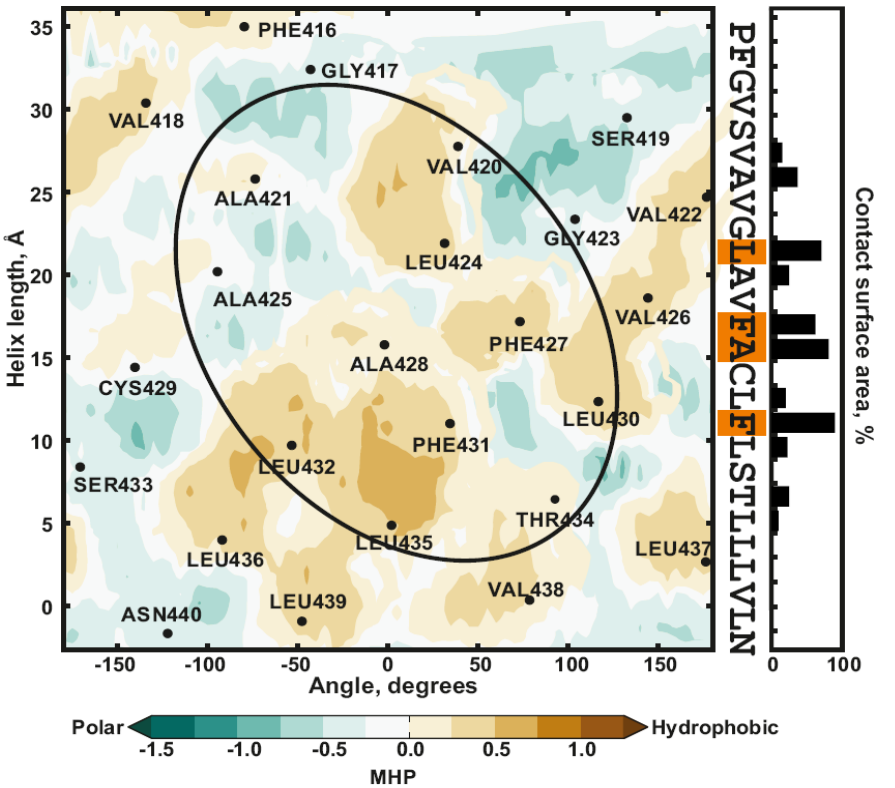
PHE416
GLY417
VAL418
SER419
VAL420
ALA421
VAL422
GLY423
LEU424
ALA425
VAL426
PHE427
ALA428
CYS429
LEU430
PHE431
LEU432
SER433
THR434
LEU435
LEU436
LEU437
VAL438
LEU439
ASN440
Helix length, Å
Angle, degrees
PFGVSVAVGLAVFACLFLSTLLVLN
Contact surface area, %
Polar
Hydrophobic
MHP

Figure S6

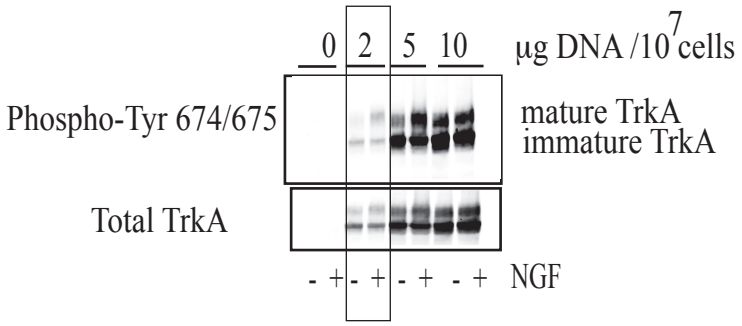
0
2
5
10
μg DNA /10^7 cells
Phospho-Tyr 674/675
mature TrkA
immature TrkA
Total TrkA
- + - + - + - + NGF

Figure S7

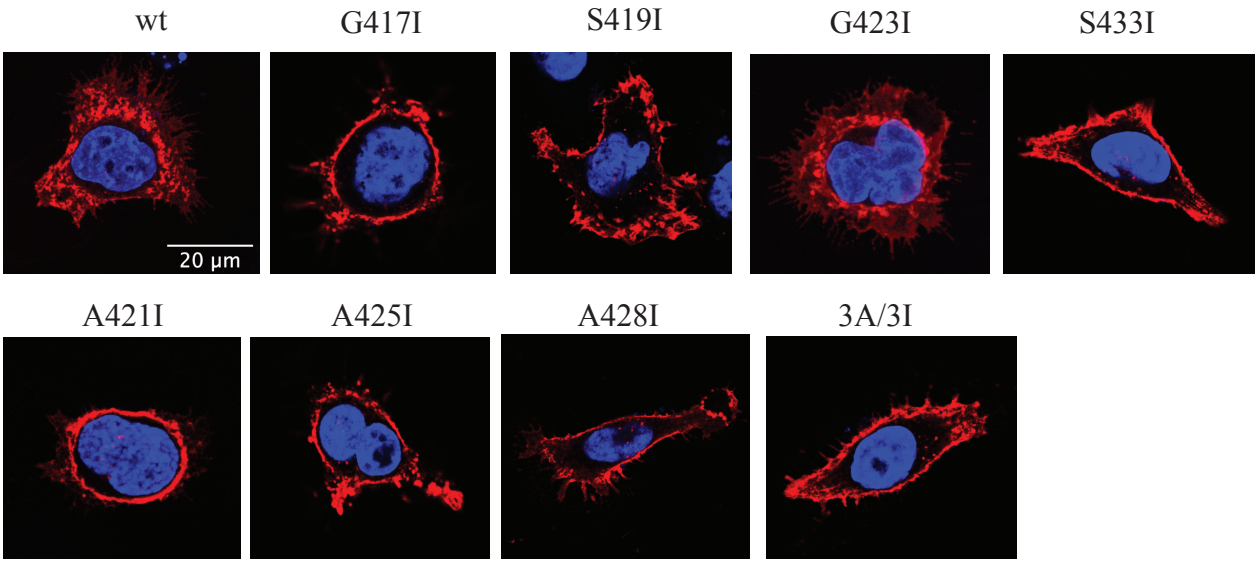

Figure S8

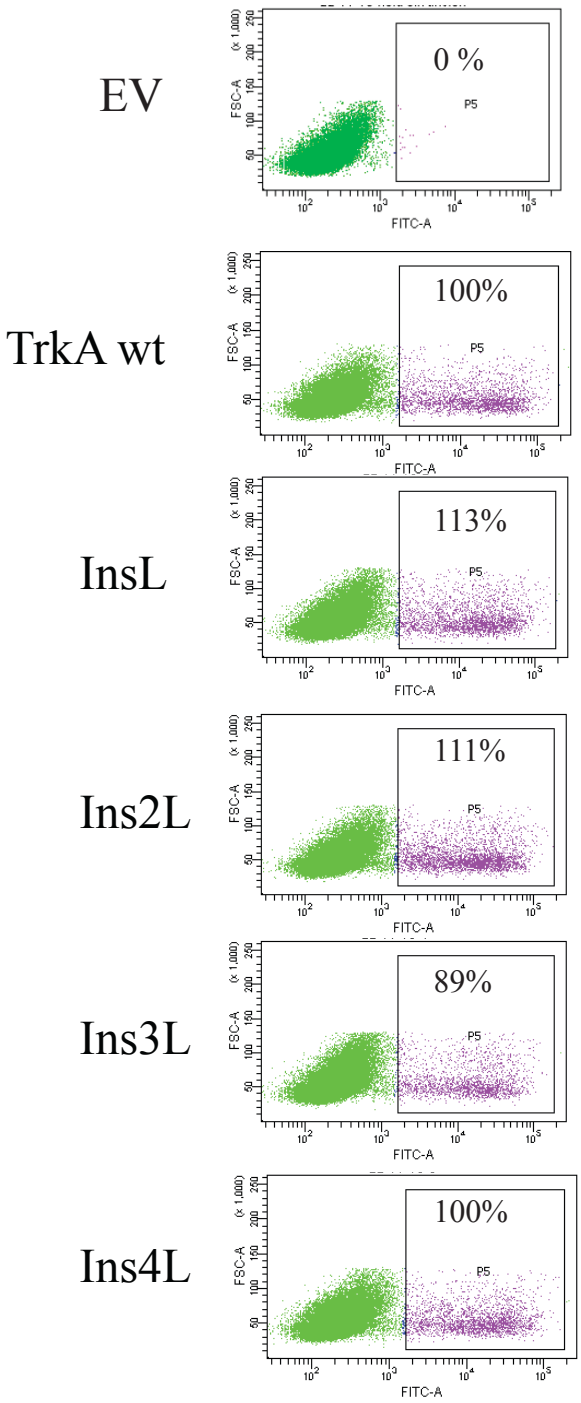
EV
0 %
P5
TrkA wt
100%
P5
InsL
113%
P5
Ins2L
111%
P5
Ins3L
89%
P5
Ins4L
100%
P5
FSC-A
(x 1,000)
FITC-A